The Journal of Immunology

RESEARCH ARTICLE | JUNE 01 2022

miR-146a Maintains Immune Tolerance of Kupffer Cells and Facilitates Hepatitis B Virus Persistence in Mice

Yongai Liu; ... et. al

J Immunol (2022) 208 (11): 2558–2572.
https://doi.org/10.4049/jimmunol.2100618

miR-146a Maintains Immune Tolerance of Kupffer Cells and Facilitates Hepatitis B Virus Persistence in Mice

Yongai Liu,*,† Lijuan Qin,*,† Jiuru Wang,*,† Xialin Xie,*,† Yu Zhang,‡ Changfei Li,*,† Zeliang Guan,*,† Liyuan Qian,§ Lizhao Chen,*,† Jun Hu,* and Songdong Meng*,†

Kupffer cells (KCs), the largest tissue-resident macrophage population in the body, play a central role in maintaining a delicate balance between immune tolerance and immunity in the liver. However, the underlying molecular mechanism remains elusive. In this study, we show that KCs express high levels of miR-146a, which is under control of the PU.1 transcription factor. miR-146a deficiency promoted KCs differentiation toward a proinflammatory phenotype; conversely, miR-146a overexpression suppressed this phenotypic differentiation. We found that hepatitis B virus (HBV) persistence or HBV surface Ag treatment significantly upregulated miR-146a expression and thereby impaired polarization of KCs toward a proinflammatory phenotype. Furthermore, in an HBV carrier mouse model, KCs depletion by clodronate liposomes dramatically promoted HBV clearance and enhanced an HBV-specific hepatic $CD8^+$ T cell and $CD4^+$ T cell response. Consistent with this finding, miR-146a knockout mice cleared HBV faster and elicited a stronger adaptive antiviral immunity than wild-type mice. In vivo IL-12 blockade promoted HBV persistence and tempered the HBV-specific CTL response in the liver of miR-146a knockout mice. Taken together, our results identified miR-146a as a critical intrinsic regulator of an immunosuppressive phenotype in KCs under inflammatory stimuli, which may be beneficial in maintenance of liver homeostasis under physiological condition. Meanwhile, during HBV infection, miR-146a contributed to viral persistence by inhibiting KCs proinflammatory polarization, highlighting its potential as a therapeutic target in HBV infection. *The Journal of Immunology*, **2022, 208: 2558–2572.**

The liver is a key frontline immune organ, with a propensity toward immune tolerance rather than immunity to Ags in the unique hepatic microenvironment (1, 2). Hepatotropic pathogens, including hepatitis B virus (HBV) and hepatitis C virus, therefore tend to establish persistent infection in the immune-tolerant liver microenvironment (3, 4). Kupffer cells (KCs) are the largest population of innate immune cells in the liver, representing ~80–90% of all tissue-resident macrophages and 35% of hepatic nonparenchymal cells (NPCs) (5, 6). They are immobile macrophages adherent to liver sinusoidal endothelial cells and are directly exposed to molecules and lymphocytes from blood, displaying highly heterogeneous subsets with characterized surface makers (5, 7–10). Due to their abundance and ideal location, KCs are central players in scavenging and capturing gut-derived microbial products, detecting and presenting Ags and maintaining homeostasis and liver immune tolerance (2, 5).

Under resting conditions, KCs constitutively express programmed death-ligand 1 (PD-L1) and show low levels of MHC class II (MHC-II) and costimulatory molecules such as CD40, CD80, and CD86, suggesting their poor capacity to stimulate allogeneic T cells (11, 12). Of note, they promote the development of regulatory T cells (Tregs) by producing IL-10 and TGF-β (13, 14). Moreover, You et al. (11) found that KCs in the steady state can secrete PGE_2 and 15-deoxy-$\Delta^{12,14}$-PGJ_2, which can directly inhibit Ag-specific $CD4^+$ T cell proliferation and activation. KCs can be activated by various damage-associated molecular patterns and pathogen-associated molecular patterns, as well as reactive oxygen species and hypoxia-inducible factor 1α in live diseases, triggering TLR/MyD88 signaling and inflammasome activation (15). Under different stimulation conditions, the polarization of macrophages can be roughly divided into proinflammatory M1 polarization and anti-inflammatory M2 polarization (16, 17). M1 polarization is characterized by the expression of high levels of proinflammatory factors, including TNF-α, IL-1β, IL-12, and inducible NO synthase (iNOS). Upregulated MHC-II, CD86, and CD80 on cell membranes are also the markers of macrophage M1 polarization. M2 polarization is characterized by high expression of immunosuppressive factors, including Mrc-1, CD163, and TGF-β (16). Similar to other macrophages,

*Key Laboratory of Pathogenic Microbiology and Immunology, Institute of Microbiology, Chinese Academy of Sciences, Beijing, China; †University of Chinese Academy of Sciences, Beijing, China; ‡Department of Pathology and Hepatology, The Fifth Medical Center, Chinese PLA General Hospital, Beijing, China; and §Beijing Key Laboratory of Environmental and Viral Oncology, College of Life Science and Bio-Engineering, Beijing University of Technology, Beijing, China

ORCID: 0000-0001-5670-1533 (S.M.)

Received for publication June 25, 2021. Accepted for publication March 23, 2022.

This work was supported by Strategic Priority Research Program of the Chinese Academy of Sciences Grant XDB29040000, National Natural Science Foundation of China Grants 81761128002, 81621091, 81871297, 81672815, 32070163, and 31700803, and by an Industrial Innovation Team grant from the Foshan Industrial Technology Research Institute.

Y.L. and J.H. designed and performed the experiments, analyzed and interpreted data, and prepared the manuscript. L. Qin, J.W., X.X., and Y.Z. performed the experiments and analyzed the data. C.L., Z.G., L. Qian, and L.C. provided reagents and reviewed the manuscript. S.M. conceived the study, designed the experiments, supervised the project, and prepared the manuscript.

The nucleotide sequence data presented in this article have been submitted to the National Center for Biotechnology Information Sequence Read Archive under accession number PRJNA695447.

Address correspondence and reprint requests to Prof. Songdong Meng and Dr. Jun Hu, Key Laboratory of Pathogenic Microbiology and Immunology, Institute of Microbiology, Chinese Academy of Sciences, Beijing, China. E-mail addresses: mengsd@im.ac.cn (S.M.) and hujun579@126.com (J.H.)

The online version of this article contains supplemental material.

Abbreviations used in this article: AAV, adeno-associated virus; anti-HB, anti-HBsAg Ab; CHB, chronic hepatitis B; ChIP, chromatin immunoprecipitation; DC, dendritic cell; HBcAg, HBV core Ag; HBeAg, HBV e Ag; HBsAg, HBV surface Ag; HBV, hepatitis B virus; HBVtg, HBV transgenic; HDI, hydrodynamic injection; iNOS, inducible NO synthase; KCs, Kupffer cells; MHC-II, MHC class II; miR/miRNA, microRNA; NC, negative control; NPCs, nonparenchymal cells; PD-L1, programmed death-ligand 1; PMs, peritoneal macrophages; qPCR, quantitative PCR; qRT-PCR, quantitative RT-PCR; si-, small interfering RNA; Treg, regulatory T cell; WT, wild-type;

activated KCs generally tend to undergo proinflammatory (M1) or anti-inflammatory (M2) polarization. Nogo-B, an endoplasmic reticulum–resident protein, was found to increase alcoholic liver disease severity by promoting M1 polarization and suppressing M2 polarization in KCs (18). In alcoholic and nonalcoholic fatty liver disease patients or mouse models, proinflammatory KCs associate to more severe liver lesions, and anti-inflammatory KCs limit liver injury through secreted IL-10 (19). In ischemia-reperfusion injury, peroxisome proliferator–activated receptor-γ induces KCs to polarize to the M2 phenotype, whereas hyperglycemia-induced sphingosine-1-phosphate signaling and sphingosine-1-phosphate receptor 3 signaling promote M1 polarization and inhibit M2 polarization (20). In addition, KCs may be induced to express PD-L1 or secret IL-10 through TLR2 by HCV core protein or hepatitis B core Ag, resulting in suppression of antiviral IFN-α/β responses, germinal center formation, and impairment of the humoral immunity and HBV-specific $CD8^+$ T cell responses (13, 21–23). Although multiple main regulators and several signaling pathways mediating macrophage polarization have been uncovered (16, 17), the intrinsic factors that control the tolerogenic function of KCs to maintain liver homeostasis remain largely ambiguous, especially under physiological conditions.

MicroRNAs (miRs/miRNAs) are single-stranded, 20- to 24-nt-long, noncoding RNA molecules that regulate gene expression at the post-transcriptional level (24). Several miRNAs, including miR-155, miR-181, miR-31, and miR-146a, are emerging as pivotal regulators in both adaptive and innate immunity, regulating development, differentiation, and function of macrophages, NK cells, and T cells (25–30). Although multiple miRNAs, including let-7c, miR-21, miR-19a, miR-33, miR-146a, miR-155, and miR-233, have been shown to clearly affect macrophage development, polarization, and activation, the role of miRNAs during KCs polarization was largely unknown until now (16). In this study, we aim to identify key endogenous miRNAs by miRNA comparative profiling that play an indispensable role in maintaining immune hyporesponsiveness of KCs. These results could shed light on mechanism of miRNA-mediated KCs polarization during hepatotropic virus infection that may provide innovative therapeutic approaches.

Materials and Methods

Materials

An HBV core–derived $CD8^+$ epitope (core 93–100: MGLKFRQL) was synthesized by GL Biochem (Shanghai, China). Recombinant HBV surface Ag (HBsAg) (A2 subtype) was a gift from Sinovac Biotech (Beijing, China), which was produced from *Hansenula polymorpha* with purity >99% and the level of endotoxin <5 endotoxin units/ml. Recombinant HBV core Ag (HBcAg) (catalog no. B501N003) and hepatitis B e Ag (HBeAg) (catalog no. B401N001) were purchased from Key-Bio Biotech (Beijing, China), which were produced and purified from an *Escherichia coli* system with purity ≥95%. The following materials were obtained from the suppliers as listed: $H\text{-}2K^b$–restricted HBV core tetramer (MGLKFRQL-PE; MBL International, catalog no. TS-M537-1), $OVA_{323\text{-}339}$ peptide (MedChemExpress, catalog no. HY-P0286), RPMI 1640 (HyClone, catalog no. SH30809.01), DMEM (Corning Life Sciences, catalog no. 10-017-CV), FBS (Corning Life Sciences, catalog no. 35-081-CV), ampicillin sodium (Amresco, catalog no. 0339), streptomycin sulfate (Amresco, catalog no. 0382), HBSS (Corning, catalog no. 21-022-CVR), PBS (Corning Life Sciences, catalog no. 21-031-CVR), HEPES (Vetec, catalog no. V900477), EGTA (Yeasen, catalog no. 60339ES60), $CaCl_2$ (Sigma-Aldrich, catalog no. C7902), IL-2 (PeproTech, catalog no. AF-212-12-20), 100 μm cell strainer (BD Falcon, catalog no. 352360), 40 μm cell strainer (BD Falcon, catalog no. 352340), and 70 μm cell strainer (BD Falcon, catalog no. 352350).

Cell line

Huh7 cells were maintained in the laboratory. Transfections were performed using Lipofectamine 3000 reagent (Invitrogen, catalog no. L3000015).

Mice

Male C57BL/6 mice (6–8 wk of age) were purchased from Vital River Laboratories (Beijing, China) and SPF (Beijing, China). miR-146a$^{-/-}$ mice (B6.Cg-*Mir146*$^{tm1.1Bal}$/J, catalog no. JAX: 016239) were purchased from The Jackson Laboratory (Bar Harbor, ME). HBV transgenic (HBVtg) BABL/c mice were purchased from Transgenic Engineering Lab, Infectious Disease Center (Guangzhou, China). To generate miR-146a$^{-/-}$ HBVtg mice, the miR-146a$^{-/-}$ C57BL/6 mice were backcrossed to HBVtg BABL/c mice for 15 generations. OT-II mice (B6.Cg-Tg(TcraTcrb)425Cbn/J, The Jackson Laboratory, catalog no. JAX: 004194) were a gift from Prof. Beinan Wang (Institute of Microbiology, Chinese Academy of Sciences). All mice were raised in a special pathogen–free facility. All animal experiments were carried out strictly according to the guidelines established by the Research Ethics Committee of the Institute of Microbiology, Chinese Academy of Sciences (permit no. PZIMCAS2011001).

HBV-carrier mouse model

The p–adeno-associated virus (p-AAV)/HBV1.2 plasmid was purified by the endo-free plasmid maxi kit (Qiagen, catalog no. 12362). The HBV-carrier mouse model was established by hydrodynamic injection (HDI) of 6 μg of p-AAV/HBV1.2 plasmid as previously described (31). The serum specimens were assayed for HBsAg, HBeAg, anti– anti-HBsAg Ab (anti-HBs), or HBV genomic DNA at the indicated time points after injection. The livers of mice were preserved in 10% neutral buffered formalin for immunohistochemical analysis.

KCs depletion

Mice were injected via the tail vein with 5 mg/ml clodronate encapsulated with liposomes in a dose of 10 μl per gram of mouse body weight 40–48 h before HDI of p-AAV/HBV1.2 plasmid (32). An equal volume of PBS-liposomes was used as a negative control.

IL-12 blockade

In IL-12p75 depletion experiments, 6- to 7-wk-old miR-146a$^{-/-}$ C57BL/6 male mice were administered by i.p. injection with 1 mg of rat anti-mouse IL-12p75 Ab (Bio X Cell, catalog no. BE0233, clone R2-9A5) or isotype control Ab (Bio X Cell, catalog no. BE0090, clone LTF-2) 2 d before the p-AAV/HBV1.2 plasmid HDI and with 500 μg on days 2, 7, and 12 after plasmid HDI.

Liver perfusion

Mice were anesthetized with i.p. administration of the appropriate amount of 4% chloral hydrate. The inferior vena cava was cannulated and the portal vein was opened for drainage (33). The liver was perfused with HBSS-EGTA (0.5 mM, supplemented with 15 mM HEPES, 100 U/ml ampicillin, 100 μg/ml streptomycin sulfate [pH 7.4]) prewarmed in 37°C at 2.5 ml/min for 8 min and followed by perfusion with prewarmed HBSS-$CaCl_2$ (5 mM, supplemented with 15 mM HEPES, 100 U/ml ampicillin, 100 μg/ml streptomycin sulfate [pH 7.4]) containing 0.35 mg/ml collagenase (Sigma-Aldrich, catalog no. C5138) and 40 μg/ml trypsin inhibitor (Sigma-Aldrich, catalog no. T7378) at 2.5 ml/min until satisfactory digestion was achieved.

KCs isolation

Once liver perfusion was completed, the gallbladder was immediately removed. The liver was removed from the abdominal cavity as one piece and was placed in a 50 ml centrifuge tube containing 50 ml of ice-cold RPMI 1640 supplemented with 3% heat-inactivated FBS, 100 U/ml ampicillin, 100 μg/ml streptomycin sulfate, and 20 μg/ml DNase I (Sigma-Aldrich, catalog no. 5025). The perfused liver tissue was gently dispersed in a 100 mm cell culture–treated plate using a pair of sterile straight-pointed ophthalmic forceps within 6 min in a hood. A single-cell suspension was filtered through a 100 μm cell strainer (BD Falcon, catalog no. 352360). The cells were centrifuged at 50 × *g* for 3 min to pellet the hepatocytes. The supernatant enriched with NPCs was transferred into a new 50 ml centrifuge tube and kept on ice for a maximum period of 3 h to avoid affecting cell viability. The perfusion procedure was repeated on several mice when needed. The NPCs were centrifuged three more times at 50 × *g* for 2 min per each at 4°C. After each centrifugation, the supernatant was collected and the hepatocyte pellets were discarded. Then, the NPCs were centrifuged at 500 × *g* for 7 min at 4°C. The pellet from one mouse was resuspended in 4 ml of ice-cold RPMI 1640 supplemented with 3% heat-inactivated FBS and placed on ice during the preparation of a 25–50% Percoll gradient. Then, the NPCs solution was loaded on the gradient and centrifuged at 850 × *g* for 15 min at 4°C without brake. The KCs fraction located at the interface of the 25–50% Percoll layer was collected carefully into a new 15 ml centrifuge tube and washed twice by adding RPMI 1640 supplemented with 3% heat-inactivated FBS to a final

volume of 14.5 ml and centrifuging at 1500 rpm for 10 min at 4°C. The pellet cells from one mouse were resuspended in 2 ml of prewarmed RPMI 1640 supplemented with 10% heat-inactivated FBS, 100 U/ml ampicillin, and 100 μg/ml streptomycin sulfate and plated into 12-well cell culture–treated plates at 1 ml per well. The cells were washed three times with prewarmed low-endotoxin PBS after incubated in a 37°C, saturated humidity, 5% CO_2 cell incubator for 16 min to remove the nonadherent cells. The adherent cells were added fresh and prewarmed RPMI 1640 supplemented with 10% heat-inactivated FBS, 100 U/ml ampicillin, and 100 μg/ml streptomycin sulfate at 1 ml per well. The adherent cells were primary KCs with purity >80% (Supplemental Fig. 1G). The KCs were rested for 24 h in an incubator for following treatment. The KCs isolated by Percoll gradient were used in experiments of quantitative RT-PCR (qRT-PCR), Western blotting, flow cytometry, and ELISA.

Isolation of peritoneal macrophages

C57BL/6 mice were rested at least 7 d at a specific pathogen–free facility before starting the experiment. Eight- to 10-wk-old male mice were sacrificed carefully by cervical dislocation, avoiding abdominal bleeding and disinfecting the skin with 70% alcohol. We discarded the mice that bled in the peritoneal cavity. Peritoneal macrophages (PMs) were harvested by peritoneal lavage. Ten microliters of ice-cold RPMI 1640 supplemented with 10% heat-inactivated FBS was injected into the peritoneal cavity, after which the abdomen of each mouse was gently massaged for 2 min. Lavage fluid was drawn with a 10-ml syringe after 20–30 min of incubation. The peritoneal cells suspension was centrifuged at 450 × *g* for 10 min at 4°C. The pellet was washed twice with ice-cold RPMI 1640. After the last wash, cells were then resuspended in prewarmed RPMI 1640 supplemented with 10% heat-inactivated FBS, 100 U/ml ampicillin, and 100 μg/ml streptomycin sulfate. The peritoneal cells from one mouse were plated in one well of a six-well cell culture–treated plate. The plate was incubated in 37°C, 5% CO_2, saturated humidity cell incubator for 2–3 h. We then washed the wells twice with prewarmed PBS, discarded the nonadherent cells, and added 2 ml of fresh RPMI 1640 complete medium to each well. The PMs can be used for downstream experiments after 24 h of incubation.

MACS

The mouse hepatic $CD8^+$ T cells, $CD4^+$ T cells, dendritic cells (DCs), and NK cells for quantitative PCR (qPCR) were purified using a corresponding MACS kit (STEMCELL Technologies, catalog nos. 19853, 19852, 18780, and 19855, respectively) according to the manufacturer's instructions. The KCs for chromatin immunoprecipitation (ChIP), RNA sequencing, and coculture with OT-II naive $CD4^+$ T cells were purified by MACS with anti-F4/80 MicroBeads (UltraPure, mouse; Miltenyi Biotec, catalog no. 130-110-443) generally as previously described (34). In brief, the perfused liver was dispersed in a 100 mm cell culture–treated plate within 6 min. The single-cell suspension was filtered through a 100 μm sterile cell strainer and centrifuged at 50 × *g* for 5 min at 4°C to pellet the hepatocytes. The supernatant was carefully collected and centrifuged at 300 × *g* for 10 min at 4°C to pellet the NPCs. The NPCs were sequentially washed once with ice-cool low-endotoxin PBS and MACS buffer (Miltenyi Biotec, catalog no. 130-091-222) supplemented with 0.5% BSA (Miltenyi Biotec, catalog no. 130-091-376). The following operation for KCs isolation was strictly in accordance with the manufacturer's instructions. KCs were resuspended with RPMI 1640 supplemented with 10% heat-inactivated FBS, 100 U/ml ampicillin, and 100 μg/ml streptomycin sulfate and plated into 12-well cell culture–treated plates at a density of 1×10^6 cells/ml. After 30 min of incubation at 37°C, cells were washed with prewarmed low-endotoxin PBS three times and prewarmed RPMI 1640 supplemented with 10% heat-inactivated FBS, 100 U/ml ampicillin, and 100 μg/ml streptomycin sulfate was added. The KCs were rested for 24 h in a 37°C, saturated humidity, 5% CO_2 cell incubator before collecting the sample. The splenic $OVA_{323–339}$ peptide–specific naive $CD4^+$ T cells were isolated using a MACS kit (STEMCELL Technologies, catalog no. 19765) from splenocytes of OT-II mice.

Isolation of hepatic mononuclear cells

We isolated liver mononuclear cells using the modified method of in situ collagenase digestion generally as previously described (35). Briefly, the liver was perfused with HBSS-EGTA (0.5 mM, supplemented with 15 mM HEPES, 100 U/ml ampicillin, and 100 μg/ml streptomycin sulfate [pH 7.4]) prewarmed at 37°C at 2.5 ml/min for 8 min and followed by prewarmed HBSS-$CaCl_2$ (5 mM, supplemented with 15 mM HEPES, 100 U/ml ampicillin, and 100 μg/ml streptomycin [pH 7.4]) containing 0.35 mg/ml collagenase (Sigma-Aldrich, catalog no. C5138) and 40 μg/ml trypsin inhibitor (Sigma-Aldrich, catalog no. T7378) at 2.5 ml/min until satisfactory digestion was achieved. The liver was then quickly removed, shred with a pair of forceps in a 100 mm cell culture–treated plate, and filtered through a 70 μm nylon cell strainer. The sample was suspended in ice-cold RPMI 1640 supplemented with 2% heat-inactivated FBS and centrifuged at 50 × *g* for 1 min at 4°C to discard the hepatocyte pellets, after which the NPCs-enriched supernatant was centrifuged at 500 × *g* for 8 min at 4°C. The pellet was suspended in 25 ml of 33.75% sterile Percoll. The liver mononuclear cells were then isolated by centrifugation at 700 × *g* for 7 min at room temperature without brake. The liver mononuclear cells were pelleted at the bottom of the 50 ml centrifuge tube with a conical bottom. We then carefully aspirated and discarded the undesirable cells on top of the Percoll gradient and suspended the pellet with 4 ml of 1× RBC lysis buffer (Beyotime, catalog no. C3702) and incubated it at room temperature for 4 min and washed three times with cold PBS containing 2% heat-inactivated FBS at 4°C, with centrifugation at 500 × *g* for 5 min after each wash. After the first wash, cells were filtered through a 40 μm nylon cell strainer and, after the last wash, cells were resuspended in 1 ml of PBS containing 2% heat-inactivated FBS and counted.

Isolation of hepatic lymphocytes

Hepatic lymphocytes were isolated as previously described (36). Livers were passed through a 200G stainless steel mesh. After washing once with PBS, the cells were resuspended in 40% Percoll and then gently overlaid on 70% Percoll and centrifuged at 2400 rpm for 30 min at room temperature. Hepatic lymphocytes were collected from the interface and washed twice in PBS.

miRNA sequencing and analyses

The total RNA was extracted from the KCs or PMs using TRIzol reagent (Invitrogen) according to the manufacturer's instructions. The transcriptome analysis was undertaken by Shanghai Majorbio Bio-pharm Biotechnology (Shanghai, China). The nucleotide sequence data were deposited in the National Center for Biotechnology Information Sequence Read Archive (https://www.ncbi.nlm.nih.gov/sra/?term=PRJNA695447) under accession number PRJNA695447. The RNA sequencing results of both KCs and PMs were compared with miRNAs in the miRBase database (http://www.mirbase.org) to identify miRNAs that were differentially expressed between these two cell types. Significantly expressed miRNAs were filtered according to a fold change >2 or <0.5.

Chromatin immunoprecipitation

The SimpleChIP enzymatic chromatin immunoprecipitation (ChIP) kit with magnetic beads (Cell Signaling Technology, catalog no. 9003S) was used according to the manufacturer's protocol. In brief, PMs or KCs were treated with 1% formaldehyde for 10 min at room temperature. Glycine (final concentration 125 mM) was added to the media and incubated with shaking for 5 min at room temperature to quench cross-linking of formaldehyde. Then, the cells were washed twice with ice-cold PBS. The cells were scraped thoroughly with a rubber cell scraper and transferred to a 1.5 ml centrifuge tube followed by a centrifugation at 700 × *g* for 5 min at 4°C. Then, the pelleted cells were lysed with buffer A for 10 min on ice to release nuclei. The nuclei were pelleted by centrifugation at 2000 × *g* for 5 min at 4°C. The nuclei were resuspended in ice-cold buffer B and treated with micrococcal nuclease for 20 min at 37°C to digest the chromatin DNA to a length of ~150–900 bp. Then, the reaction of enzyme was stopped by EDTA. The nuclei were pelleted by centrifugation at 16,000 × *g* for 1 min at 4°C and resuspended in 100 μl of 1× ChIP buffer supplemented with protein inhibitor mixture per IP sample followed by incubation on ice for 10 min. The nuclei were sonicated with three sets of 20 s pulses at an interval of 30 s on ice. The sheared chromatin was collected by centrifugation at 9400 × *g* for 10 min at 4°C. Abs (5 μg) each against histone 3 (positive control), PU.1, or normal IgG control were used for IP with 10 μg of sheared chromatin. The IP samples were incubated overnight at 4°C with rotation. Then, 30 μl of ChIP-grade protein G magnetic beads per IP sample were added and incubated for 2 h at 4°C with rotation. The protein G pellet was washed sequentially with low-salt and high-salt ChIP buffer. The chromatin was eluted from Ab/protein G magnetic beads with 150 μl of ChIP elution buffer per IP sample for 30 min at 65°C with gentle vortex. Cross-links were reversed by adding 6 μl of 5 μM NaCl, 2 μl of proteinase K per chromatin supernatant sample and incubated for 2 h at 65°C. The chromatin DNA was purified using spin columns and eluted with 50 μl of DNA elution buffer per spin column. The eluted DNA fragments were subjected to real-time PCR with SYBR Green. The primers used in the experiments were as follows: miR-146a, forward, 5′-CCA CCT TAA AGC CAG CAG AG-3′, reverse, 5′-CCT GAC CAG CAC TTC CTC AG-3′; PU.1, forward, 5′-AGG CAG AGC ACA CAT GCT TC-3′, reverse, 5′-CTT CTG GGC AGG GTC AGA GT-3′; flt3, forward, 5′-TTT GCA CTC GTA GCA AAT GG-3′, reverse, 5′-GTT CAG CTG CCA AAG AGA GG-3′.

Table I. Primers sequences for qRT-PCR

Gene	Forward Primer (5′→3′)	Reverse Primer (5′→3′)
IL-1β	GAAATGCCACCTTTTGACAGTG	TGGATGCTCTCATCAGGACAG
TNF-α	CCTGTAGCCCACGTCGTAG	GGGAGTAGACAAGGTACAACCC
iNOS	GTTCTCAGCCCAACAATACAAGA	GTGGACGGGTCGATGTCAC
IL-12p40	GTCCTCAGAAGCTAACCATCTCC	CCAGAGCCTATGACTCCATGTC
IL-12p35	CAATCACGCTACCTCCTCTTTT	CAGCAGTGCAGGAATAATGTTTC
Mrc-1	CTCTGTTCAGCTATTGGACGC	TGGCACTCCCAAACATAATTTGA
IL-10	GCTGGACAACATACTGCTAACC	ATTTCCGATAAGGCTTGGCAA
Stat1	GCTGCCTATGATGTCTCGTTT	TGCTTTTCCGTATGTTGTGCT
p65	AGGCTTCTGGGCCTTATGTG	TGCTTCTCTCGCCAGGAATAC
PU.1	TTACAGGCGTGCAAAATGGAA	GACGTTGGTATAGCTCTGAATCG
Ets-1	CCCTGGGTAAAGAATGCTTCC	GCTGATGAAGTAATCCGAGGTG
GAPDH	TGACCTCAACTACATGGTCTACA	CTTCCCATTCTCGGCCTTG

Quantitative real-time PCR

The primers used in our gene expression experiments are shown in Table I. The qPCR condition was 95°C for 3 min, followed by 40 cycles of 95°C for 10 s and 60°C for 45 s. Amplification of specific transcripts was confirmed by melting curve profiles generated at the end of the PCR program. Expression levels of target genes were normalized to the expression of GAPDH and calculated based on the comparative cycle threshold (Ct) method ($2^{-\Delta\Delta Ct}$).

T cell proliferation assays

For Ag-restricted T cell stimulation assays, 2×10^5 KCs pulsed with $OVA_{323–339}$ peptide were cultured with 1×10^6 naive $CD4^+$ OVA-TCR T cells from OT-II mice for 96 h in a U-bottom 96-well plate.

Flow cytometry

The mAbs used for flow cytometry in this study are shown in Table II. For flow cytometry, 1×10^6 cells/sample were used. Cells were blocked with PBS containing 5% BSA for 30 min at 4°C and then stained with fluorochrome-conjugated Abs for surface Ags for 30 min at 4°C. For intracellular staining of cytokines, cells were fixed in 100 μl of IC (intracellular) fixation buffer (eBioscience, catalog no. 00-8222-49) for 20 min at room temperature. Then, the samples were washed twice with 1× permeabilization solution (eBioscience, catalog no. 00-8333-56) at 1.5 ml/wash/sample and centrifuged after each wash at 500 × *g* for 5 min at 4°C. After the last wash, cells were resuspended in 100 μl of 1× permeabilization solution and stained with fluorochrome-conjugated Abs for 30 min at 4°C. For transcription factor staining, cells were fixed in fixation/permeabilization buffer (eBioscience, catalog nos. 00-5123-43 and 00-5223-56) for 1 h at room temperature. Then, the samples were washed twice with 1× permeabilization solution (eBioscience, catalog no. 00-8333-56). After the last wash, cells were resuspended in 100 μl of 1× permeabilization solution and stained with fluorochrome-conjugated Abs for 30 min at 4°C. The samples were finally washed twice with PBS and resuspended in PBS for immediate analysis or in 4% polyoxymethylene for temporary storage. The samples were analyzed on a FACSCalibur flow cytometer (BD Biosciences) or LSR Fortessa flow

Table II. Abs for flow cytometry, Western blots, and immunohistochemistry

Abs	Company	Catalog No.	Clone No.
FITC anti-CD4	BioLegend		GK1.5
FITC anti-CD11b	BioLegend		M1/70
PE anti-CD3e	eBioscience		145-2C11
PE-Cy5.5 anti-CD8a	eBioscience		53-6.7
PE anti-CD25	Invitrogen		PC61.5
PE anti-F4/80	BioLegend		BM8
PE anti-CD69	BioLegend		H1.2F3
PE-Cy5 anti-CD44	BioLegend		IM7
PE-Cy7 anti-CD86	Invitrogen		GL1
PE-Cy7 anti-CD80	Invitrogen		16-10A1
Allophycocyanin anti–MHC-II	Invitrogen		M5/114.15.2
Allophycocyanin anti–IFN-γ	BioLegend		XMG1.2
Allophycocyanin anti-CD69	BioLegend		H1.2F3
Allophycocyanin anti–PD-L1	BioLegend		10F.9G2
FITC anti-CD62L	BioLegend		MEL-14
BV510 anti-F4/80	BioLegend		BM8
PE anti-CD163	BioLegend		S15049I
PerCP-Cy5.5 anti-CD206	BioLegend		C068C2
PE anti-CD4	BD Biosciences		RM4-5
Allophycocyanin anti-CD3	BioLegend		17A2
PE anti-CD19	BioLegend		6D5
PE anti-CD11c	BioLegend		N418
BV650 anti-CD4	BioLegend		GK1.5
BV421 anti–IFN-γ	BioLegend		XMG1.2
PE-Cy7 anti-NK1.1	BioLegend		S17016D
Allophycocyanin anti-B220	BioLegend		RA3-6B2
BV605 anti-CD11c	BioLegend		N418
Allophycocyanin anti-Foxp3	Invitrogen		FJK-16s
PerCP-Cy5.5 anti-CD3	BioLegend		145-2C11
BV605 anti–Ki-67	BioLegend		16A8
anti-Stat1	Cell Signaling Technology	9172S	
anti–p-Stat1	Cell Signaling Technology	9167S	
anti–p-IκBα	Santa Cruz	sc-8404	
anti-PU.1	Abcam	ab227835	
anti–β-actin	Abcam	ab8226	
anti-HBcAg	Abcam	ab17228	

cytometer (BD Biosciences). The data were further analyzed using FlowJo software (Tree Star).

Analysis of activated $CD8^+$ T and $CD4^+$ T cells

For HBV-specific $CD8^+$ T intracellular IFN-γ staining, liver lymphocytes were stimulated with 20 μg/ml HBc93-100 peptide for 18 h. For HBV-specific $CD4^+$ T intracellular IFN-γ staining, liver lymphocytes were stimulated with 10 μg/ml HBcAg for 24 h. Brefeldin A was added for the last 6 h to prevent cytokine secretion. After stimulation, cells were harvested, washed with PBS containing 2% FBS, and resuspended in the same wash buffer. To evaluate HBV-specific $CD8^+$ T cells, HBV core tetramer (MBL International, catalog no. TS-M537-1) was used according to the manufacturer's instructions. The staining of IFN-γ and the cell surface marker was performed as described above.

miRNA qPCR analysis

The primers kits for miR-146a-5p and U6 were purchased from Applied Biosystems. The U6 endogenous control was used for normalization. A TaqMan miRNA reverse transcription kit (Applied Biosystems, catalog no. 4366597) and TaqMan universal PCR master mix (Applied Biosystems, catalog no. 4304437) were used in reverse transcription and qPCR experiments. The qPCR condition was 95°C for 10 min, followed by 40 cycles of 95°C for 10 s and 60°C for 45 s.

Small interfering RNA and miRNA mimic transient transfection

miR-146a mimic, miRNA mimic negative control (NC), small interfering RNA (si-)Stat1, si-p65, and si-NC were designed by RiboBio (Guangzhou, China) and synthesized with the chemical synthesis method. The sequences of oligonucleotides used are as follows: miR-146a-5p mimics, forward, 5′-UGA GAA CUG AAU UCC AUG GGU U-3′, reverse, 5′-CCC AUG GAA UUC AGU UCU CAU U-3′; miR-NC mimic, forward, 5′-UUC UCC GAA CGU GUC ACG UTT-3′, reverse, 5′-ACG UGA CAC GUU CGG AGA ATT-3′; si-Stat1, sense, 5′-CUG UGA UGU UAG AUA AAC A-dTdT-3′, anti-sense, 5′-UGUU UAU CUA ACA UCA CAG-dTdT-3′; and si-p65, sense, 5′-GAA GAA GAG UCC UUU CAAU-dTdT-3′, anti-sense, 5′-AUUG AAA GGA CUC UUC UUC-dTdT-3′. KCs were rested for 24 h before the experiment, and medium was refreshed and cells were incubated for 12 h before nucleic acid transfection. KCs were transfected with 100 nM si-Stat1, si-p65, and si-NC or 100 nM miR-146a mimic and miRNA mimic NC for 36 h using Lipofectamine RNAiMAX (Thermo Fisher Scientific, catalog no.13778150) according to the manufacturer's instructions. The expression levels of Stat1 and p65 mRNA were detected by qPCR.

Western blotting

Western blotting was performed generally as previously described (37). Abs against Stat1 (Cell Signaling Technology, catalog no. 9172S), p-Stat1 (Cell Signaling Technology, catalog no. 58D6), p–I-κB_α (Santa Cruz, catalog no. sc-8404), PU.1 (Abcam, catalog no. ab227835), and β-actin (Abcam, catalog no. ab8226) were used.

ELISA

Serum HBsAg was measured by an ELISA kit (Shanghai Kehua Bio-engineering, Shanghai, China) according to the manufacturer's instructions. Commercial HBsAg standards were used to generate a calibration curve. The lower limit of detection for HBsAg was 0.5 ng/ml. Serum dilutions of 5- to 100-fold were used to obtain values within the linear range of the standard curve. Anti-HBs were analyzed on a precoated HBsAg plate and developed by HRP-labeled anti-mouse IgG (Zhong Shan Golden Bridge Biological Technology, Beijing, China). IL-12p75 was measured by an ELISA kit (Dakewe Biotech, Shenzhen, China).

Detection of serum HBV DNA

The total DNA of the serum samples was extracted and detected for HBV DNA by real-time PCR using an HBV DNA quantitative detection kit (Shanghai Kehua Bio-engineering, Shanghai, China) according to the manufacturer's instructions.

Immunohistochemistry

Liver samples were fixed in 10% neutral buffered formalin for at least 48 h, embedded in paraffin, and cut into 5-μm-thick sections. The slides were dewaxed in ethanol followed by Ag retrieval with 0.01 M sodium citrate with 0.05% Tween 20. Endogenous peroxidase was inactivated using 3% hydrogen peroxide. Liver sections were incubated with rabbit anti-mouse HBcAg Ab (Abcam, catalog no. ab17228), followed by biotinylated anti-rabbit IgG and streptavidin-HRP conjugate. Staining was developed with a 3,3′-diaminobenzidine kit.

Induction of bone marrow–derived DCs

Bone marrow progenitors were cultured in RPMI 1640 (supplemented with 10% heat-inactivated FBS, 100 U/ml ampicillin, and 100 μg/ml streptomycin sulfate) containing 10 ng/ml GM-CSF and 1 ng/ml IL-4. The medium was changed every 2 d. On day 7, the cells were collected for flow cytometry analysis (Supplemental Fig. 1E, right panel).

Statistical analysis

All data are expressed as the mean ± SEM. An unpaired two-tailed Student *t* test was used for statistical analyses. Log-rank tests were used to assess survival. Data were considered statistically significant when the difference reached $p < 0.05$. Significance is denoted as follows: $*p < 0.05$, $**p < 0.01$.

Data availability

Raw data are available from the National Center for Biotechnology Information Sequence Read Archive (https://www.ncbi.nlm.nih.gov/sra/?term=PRJNA695447) under accession number PRJNA695447.

Results

KCs with high abundance of miR-146a induced by PU.1 display a less proinflammatory and more anti-inflammatory phenotype

To profile miRNAs vital for controlling the tolerogenic phenotype of KCs, small RNA sequencing was performed to identify miRNAs differentially expressed between KCs and PMs, which are considered less tolerant in the steady state (38). The profiling data revealed a markedly different expression pattern of endogenous miRNAs between these two cell types. Of particular interest, miR-146a, an operator miRNA for anti-inflammation, was abundant among the miRNAs upregulated in KCs (Fig. 1A). miR-146a expression was ∼6-fold higher in KCs than in PMs (Fig. 1B). Among the hepatic immune cell populations, including NK cells, DCs, $CD4^+$ T cells, and $CD8^+$ T cells, KCs showed the highest expression of miR-146a (Fig. 1C).

The transcription of miR-146a is regulated by several transcription factors, including NF-κB, ETS-1, and PU.1 (39–41). Among them, PU.1 expression was elevated at both the mRNA and protein levels in KCs (Fig. 1D, 1E). ChIP analysis showed that PU.1 binding to the miR-146a promoter was significantly augmented in KCs compared with that in PMs (Fig. 1F), suggesting that increased PU.1 binding is responsible for the high expression of miR-146a.

As an important negative regulator of innate immune cell function, miR-146a is expressed at a lower level in monocytes polarized with M1 conditions than in those polarized with M2 conditions (42). Hence, we examined expression of proinflammatory IL-1β, iNOS, IL-12a, IL-12b, and anti-inflammatory Mrc-1 in naive KCs and PMs. As shown in Fig. 1G (left panel), much lower levels of IL-1β, iNOS, IL-12a, and IL-12b and higher levels of Mrc-1 were observed in KCs compared with PMs (all $p < 0.05$ or $p < 0.01$). Accordingly, flow cytometry analysis showed that the M2 markers CD163 (Fig. 1H) and CD206 (Fig. 1I) expression levels on naive KCs were also much higher than those on PMs, but the M1 marker CD38 expression on naive KCs was comparable to that on PMs (Fig. 1J). These results indicated that KCs were less proinflammatory and more anti-inflammatory than PMs under homeostatic conditions. In addition, under stimulation with the typical M1 polarization factor LPS, KCs also exhibited less M1 polarization compared with PMs (Fig. 1G, right panel). Taken together, it seems that abundant miR-146a in KCs plays a critical role in maintaining tolerance under homeostasis and suppressing stimuli-induced inflammatory polarization.

miR-146a inhibits KCs M1 polarization by targeting stat1 and NF-κB

To investigate the role of miR-146a in KCs M1 polarization, we isolated KCs from wild-type (WT) or miR-$146a^{-/-}$ C57BL/6 mice and analyzed the expression of M1 markers. As shown in Fig. 2A and 2C, miR-$146a^{-/-}$ KCs exhibited significantly higher levels of M1

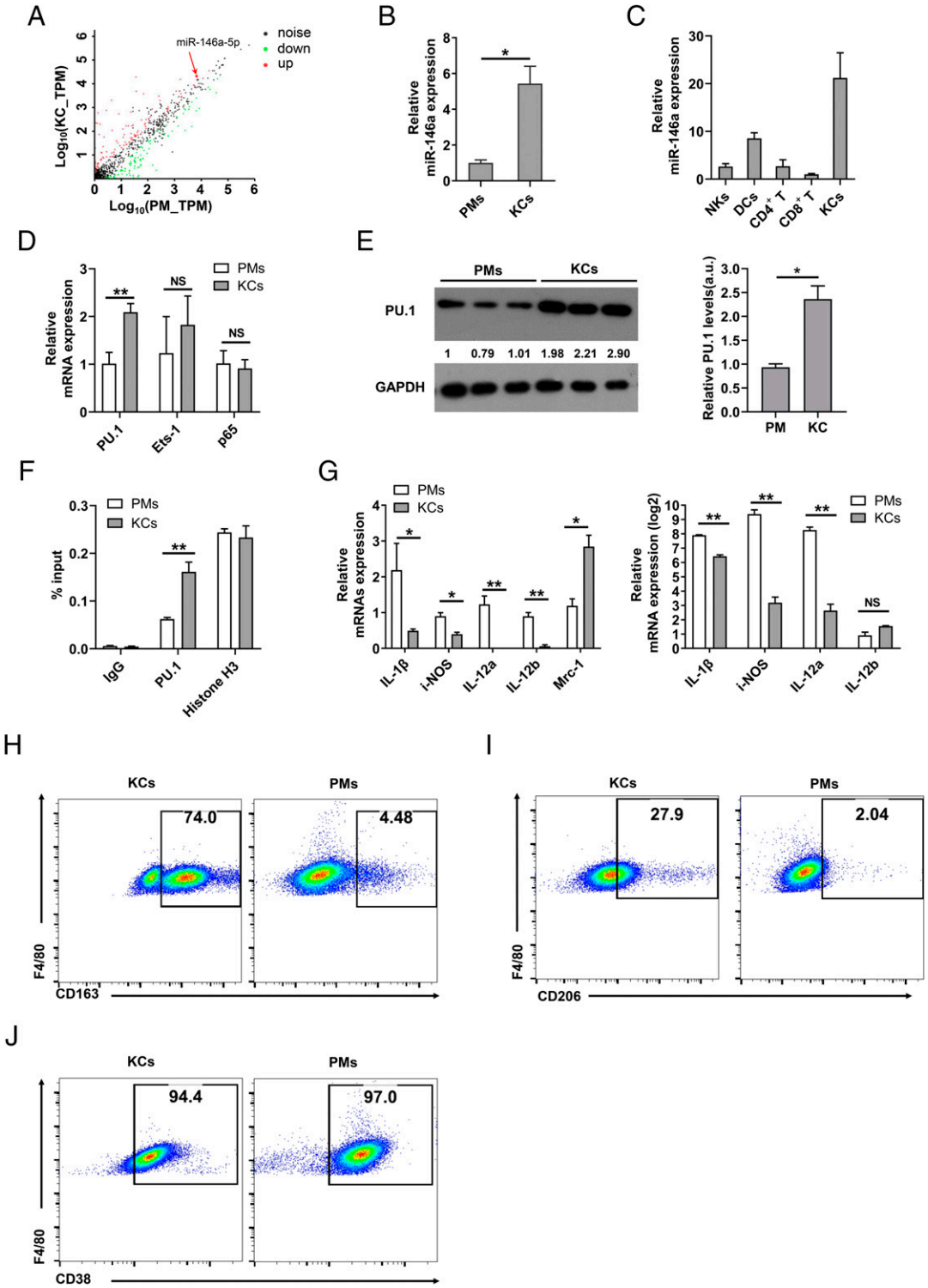

FIGURE 1. Higher miR-146a expression mediated by PH.1 in KCs than in PMs is associated with immune tolerance. (**A**) Log_{10}–log_{10} scatter plot of miRNA microarray data for PMs and KCs isolated from naive C57BL/6 mice. The values on the *y*-axis show the log base 10 of the average TPM value of miRNAs in KCs. The values on the *x*-axis show the log base 10 of the average TPM value of miRNAs in PMs. The red dots correspond to miRNAs that show a significant upregulation in KCs compared with PMs, the green dots correspond to miRNAs that show a significant downregulation in KCs compared with PMs, and the black dots correspond to miRNAs that did not show significant change between KCs and PMs. miR-146a-5p is indicated by a red arrow. The correspondent raw data are shown in Supplemental Table I. (**B**) Relative expression of miR-146a in PMs and KCs was detected by qRT-PCR. (**C**) Relative expression of miR-146a in NKs, DCs, $CD4^+$ T cells, $CD8^+$ T cells, and KCs in the liver was detected by qRT-PCR. (**D**) Relative mRNA expression of PU.1, Ets-1, and p65 was detected by qRT-PCR. (**E**) PU.1 protein expression was determined by Western blotting. (**F**) The enrichment of PU.1 in the miR-146a promoter was determined by ChIP, using IgG as a negative control and histone H3 as a positive control. (**G**) Relative mRNA expression of IL-1β, iNOS, IL-12a, IL-12b, and Mrc-1 in naive PMs and KCs was detected by qRT-PCR (left panel). Relative mRNA expression of IL-1β, iNOS, IL-12a, and IL-12b was detected by qRT-PCR in PMs and KCs after stimulation by 100 ng/ml LPS for 24 h (right panel). (**H**–**J**) The expression of CD163 (H), CD206 (I), and CD38 (J) on naive KCs and PMs was analyzed by flow cytometry. Results are expressed as the mean ± SEM (n = 3–5 mice/group). $*p < 0.05$, $**p < 0.01$, by an unpaired two-tailed Student t test. Experiments were repeated three times with similar results. a.u., arbitrary units; log_{10}(KC_TPM), the log base 10 of the average TPM value of miRNAs in KCs; log_{10}(PM_TPM), the log base 10 of the average TPM value of miRNAs in PMs; TPM, transcripts per kilobase of exon model per million mapped reads.

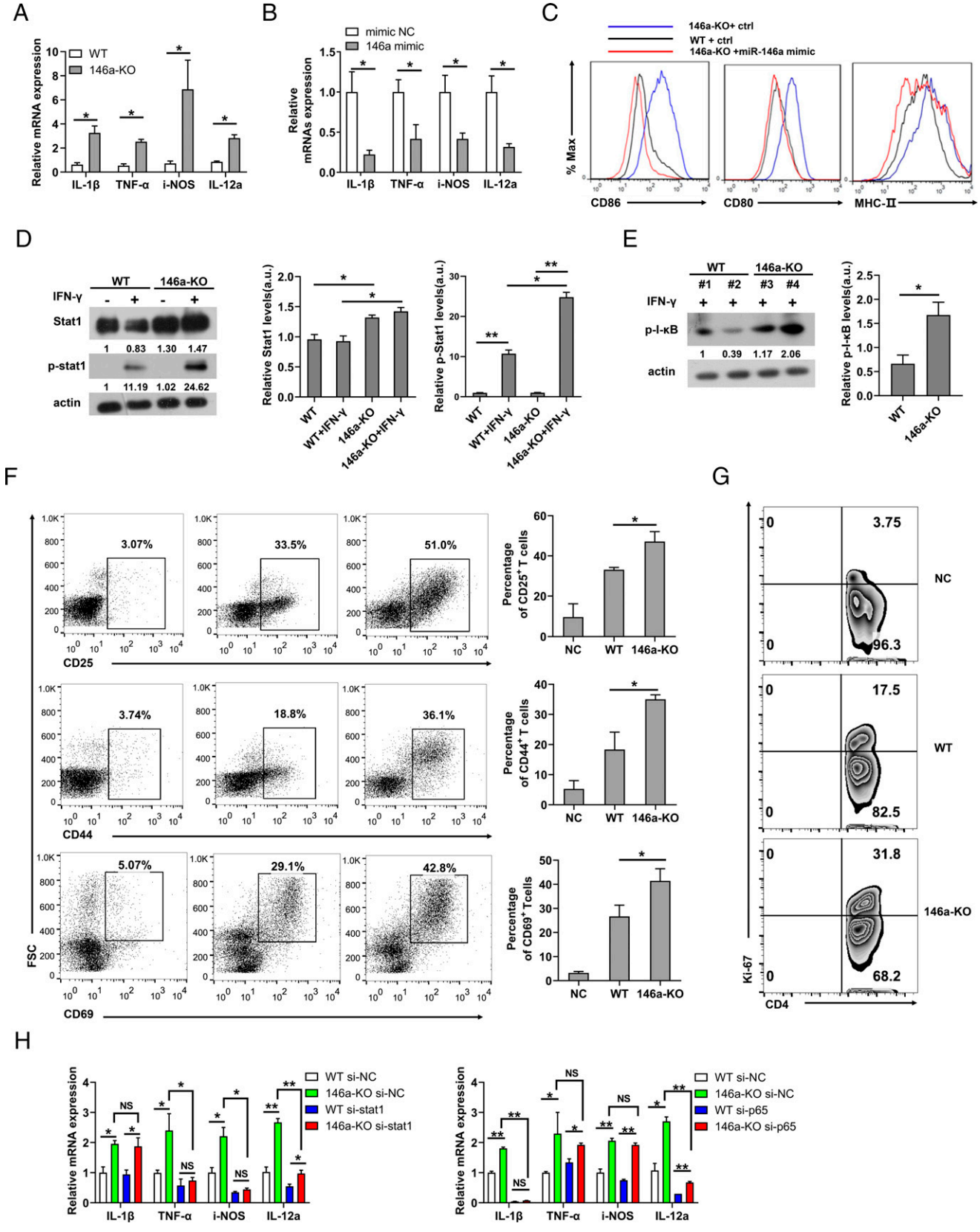

FIGURE 2. miR-146a suppresses KCs M1 polarization by targeting Stat1 and NF-κB. (**A**) Relative mRNA expression of IL-1β, TNF-α, iNOS, and IL-12a was detected by qRT-PCR in WT and 146a-KO KCs stimulated with 20 ng/ml IFN-γ and 10 ng/ml LPS for 24 h. (**B**) 146a-KO KCs were transfected with miR-146a-5p mimic or randomized oligonucleotide as a negative control for 24 h, then stimulated with 20 ng/ml IFN-γ + 10 ng/ml LPS for another 24 h. Relative mRNA expression of IL-1β, TNF-α, iNOS, and IL-12a was detected by qRT-PCR. (**C**) 146a-KO KCs were transfected with miR-146a-5p mimic for 24 h, then WT KCs, and 146a-KO KCs that transfected with miR-146a-5p mimic or not were stimulated with 20 ng/ml INF-γ + 10 ng/ml LPS for another 24 h. The expression of CD80, CD86, and MHC-II on KCs was analyzed by flow cytometry. (**D**) Western blotting analysis of Stat1 *(Figure legend continues)*

markers including IL-1β, TNF-α, iNOS, IL-12a, as well as CD80, CD86, and MHC-II compared with WT cells. Accordingly, miR-146a mimic transient transfection in miR-146a$^{-/-}$ KCs significantly decreased these M1 markers, reversing the characteristic M1 phenotype (Fig. 2B, 2C). To determine whether miR-146a deficiency can influence the ability of KCs to induce CD4$^+$ T cell differentiation, we pulsed KCs with OVA$_{323–339}$ peptide before culture with epitope-specific naive CD4$^+$ T cells from OT-II mice. Compared with WT KCs, miR-146a$^{-/-}$ KCs induced higher levels of CD4$^+$ T cell activation and proliferation, which were reflected by higher expression of CD25, CD44, CD69, and Ki-67 (Fig. 2F, 2G, Supplemental Fig. 1A). The flow cytometry gating strategy for identification of activated CD4$^+$ T cells is shown in Supplemental Fig. 1B. The purity levels of KCs and naive CD4$^+$ T cells isolated by MACS were >94% (Supplemental Fig. 1C, 1F). The percentages of contaminating monocytes (Supplemental Fig. 1C), B cells (Supplemental Fig. 1D), and DCs (Supplemental Fig. 1E) in isolated KCs were around 0.22%, 0.25%, and 0.78%, respectively, as determined by flow cytometry. Similar percentages of these contaminating immune cells were observed in WT and miR-146a$^{-/-}$ KCs. This indicates that KCs played a major role in CD4$^+$ T cell activation in the coculture experiment, although we cannot totally exclude the possibility that other cell populations, especially DCs, may partly contribute to CD4$^+$ T cell activation and proliferation.

We further explored the mechanism underlying miR-146a–driven M1 polarization repression. miR-146a represses NF-κB and Stat1 signaling by targeting IL-1R–associated kinase 1, TNFR-associated factor 6, and Stat1 (39, 43). According to the importance of NF-κB and Stat1 in macrophage M1 programming (16), we hypothesized that miR-146a regulates KCs polarization by targeting NF-κB and Stat1. Indeed, miR-146a deficiency upregulated Stat1 and NF-κB signaling in KCs upon stimulation with IFN-γ (Fig. 2D, 2E). Knockdown of Stat1 or NF-κB largely abolished the capacity of miR-146a to repress M1 polarization of KCs (Fig. 2H), indicating that miR-146a inhibits KCs M1 polarization by targeting Stat1 and NF-κB. The purity levels of KCs isolated by Percoll gradient are shown in Supplemental Fig. 1G. Stat1 si-RNA and NF-κB si-RNA knockdown efficiency levels are shown in Supplemental Fig. 1H.

HBV persistence induces miR-146a expression and decreases KCs M1 polarization by HBsAg

Next, we investigated the effect of HBV persistence on KCs M1 polarization. We employed HBVtg mice (44), a model of vertically transmitted chronic HBV infection. KCs from HBVtg mice exhibited ~2-fold higher miR-146a expression than from WT mice ($p < 0.01$) (Fig. 3A, left panel). Similar results were observed in HBV carrier mice generated by p-AAV/HBV1.2 plasmid HDI (Fig. 3A, right panel), as a model for adult chronic HBV infection (31). To elucidate which components of HBV were responsible for the upregulation of miR-146a, naive WT KCs were treated with HBsAg, HBeAg, or HBcAg, respectively. As shown in Fig. 3B, HBsAg treatment significantly promoted the expression of miR-146a. Furthermore, HBsAg-treated KCs showed higher expression of PU.1 (Fig. 3C), which might be responsible for the upregulation of miR-146a. To assess the role of HBV-induced miR-146a on KCs polarization, we generated miR-146a$^{-/-}$ HBVtg mice by backcrossing the miR-146a$^{-/-}$ C57BL/6 mice to HBVtg BABL/c mice for 15 generations. Accordingly, KCs from WT HBVtg mice tended to have an immune tolerance phenotype, downregulating proinflammatory IL-1β, TNF-α, iNOS, and IL-12a relative to those from WT littermates (Fig. 3D). In contrast, KCs from miR-146a$^{-/-}$ HBVtg mice expressed significantly higher IL-1β, TNF-α, iNOS, and IL-12a when compared with those from WT HBVtg mice (Fig. 3D). However, the expression levels of these proinflammatory mediators in KCs from miR-146a$^{-/-}$ HBVtg mice were comparable to those in miR-146a$^{-/-}$ mice. We further examined the role of HBsAg, which elevates the expression of miR-146a, in regulating the polarization of KCs. HBsAg treatment exacerbated the immune tolerance phenotype of WT KCs, exhibiting a decline of M1 marker levels (Fig. 3E, Supplemental Fig. 2), but it had no such an effect on miR-146a$^{-/-}$ KCs (Fig. 3F). Moreover, HBsAg decreased Stat1 and NF-κB signaling in WT KCs (Fig. 3G), but not in miR-146a$^{-/-}$ KCs (Fig. 3H), which is associated with M1 programming.

KCs depletion or miR-146a deficiency enhances HBV-specific T cell activation and accelerates HBV clearance in the HBV carrier mouse model

To further determine the role of KCs in immune tolerance and viral persistence, we used a well-established HBV-persistent mouse model generated by HDI of p-AAV/HBV1.2 plasmid into C57BL/6 mice. In this model, mice persistently express HBsAg without any liver pathology. We pretreated WT mice with clodronate liposome 2 d before HDI of p-AAV/HBV1.2 plasmid, which can transiently deplete KCs in mice (45). Indeed, KCs were completely depleted 2 d after i.v. injection with clodronate liposome (Fig. 4A, Supplemental Fig. 3A, 3B). Clodronate liposome treatment had no effect on the proportions of most hepatic immune cell subsets, including monocytes (Supplemental Fig. 3A, 3C), B cells (Supplemental Fig. 3A, 3D), DCs (Supplemental Fig. 3A, 3E), T cells (Supplemental Fig. 3A, 3F), and NKs (Supplemental Fig. 3A, 3H), which was consistent with previous studies (46, 47). It partially reduced hepatic NKT cells (Supplemental Fig. 3A, 3G). It has been reported that KCs-derived IL-1β plays a critical role in recruiting NKT cells into the liver (48). Thus, the reduction of hepatic NKT cells after clodronate liposome treatment was due to KCs depletion. Depletion of KCs resulted in a clearly accelerated viral clearance in WT mice, as PBS liposome–pretreated mice exhibited persistence of HBsAg and HBcAg for up to 5 wk after HDI, whereas clodronate liposome–pretreated mice showed significantly lower levels of HBsAg and undetectable HBcAg at corresponding time points (Fig. 4B, 4C). In addition, a high level of anti-HBs was detected in clodronate liposome–pretreated WT mice but not in PBS liposome–pretreated WT mice (Fig. 4D). We also analyzed hepatic HBV-specific CD8$^+$ T cells and Th1 cells 2 wk after p-AAV/HBV1.2 plasmid HDI. As shown in Fig. 4E, clodronate liposome pretreatment increased the percentage of IFN-γ–producing CD8$^+$ T cells to 6.4% in WT mice. Additionally, the percentage of

and p-Stat1 in WT and 146a-KO KCs stimulated with 20 ng/ml IFN-γ for 30 min. (**E**) Western blotting analysis of p-I-κB protein expression in WT and 146a-KO KCs stimulated with 20 ng/ml IFN-γ for 30 min. (**F** and **G**) 10 μg/ml OVA$_{323–339}$ peptide–pulsed WT or 146a-KO KCs were cultured with OVA$_{323–339}$ epitope–specific naive CD4$^+$ T cells from OT-II mice for 96 h. (F) CD4$^+$ T cells were gated and tested the expression of CD25, CD44, CD69 by flow cytometry. (G) The expression of Ki-67 in CD4$^+$ T cells was analyzed by flow cytometry. (**H**) WT and 146a-KO KCs were transfected with 100 nM Stat1 small interfering RNA (siRNA) (left panel), p65 siRNA (right panel), or negative control siRNA for 36 h, respectively, followed by treatment with 20 ng/ml IFN-γ and 10 ng/ml LPS for 24 h. Relative mRNA expression of IL-1β, TNF-α, iNOS, and IL-12a was detected by qRT-PCR. The experiments were repeated three times with similar results. Data are expressed as mean ± SEM of three mice/group. *$p < 0.05$, **$p < 0.01$, by an unpaired two-tailed Student t test. 146a-KO, miR-146a$^{-/-}$; a.u., arbitrary units; Ctrl, control; NC, negative control; WT, wild-type.

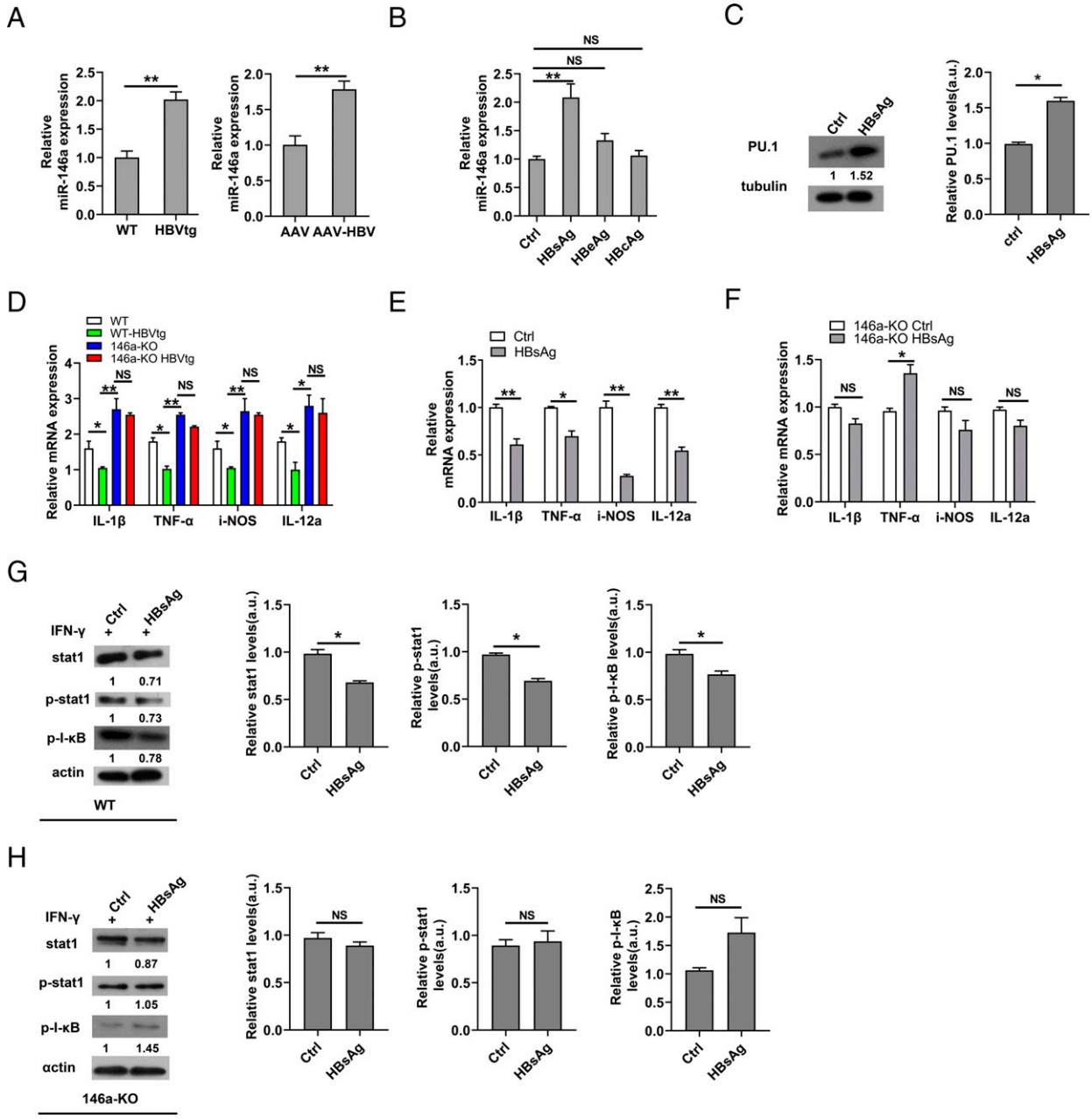

FIGURE 3. HBV infection decreases KCs M1 polarization by inducing miR-146a. (**A**) miR-146a relative expression in KCs were detected by qRT-PCR. Left panel, KCs were isolated from WT or HBVtg mice. Right panel, Mice with 6 μg/ml p-AAV-HBV1.2 plasmid were hydrodynamically injected into C57BL/6 mice to generate HBV carrier mice. PAAV-null plasmid was used as a negative control. KCs were isolated 14 d after HDI. (**B**) miR-146a relative expression in KCs was detected by qRT-PCR. KCs were isolated from healthy WT C57BL/6 mice and plated in 12-well plates at 10^6 cells/well. Twenty-four hours after plating, KCs were treated with 10 μg/ml HBeAg, 10 μg/ml HBsAg, or 10 μg/ml HBcAg, respectively, for 24 h. (**C**) Naive WT KCs were isolated and plated as in (B) and treated with 10 μg/ml HBsAg for 24 h. PU.1 protein expression in KCs was determined by Western blotting. (**D**) Relative expression of IL-1β, TNF-α, iNOS, and IL-12a was determined by qRT-PCR in KCs from WT, WT-HBVtg, 146a-KO, or 146a-KO-HBVtg mice. (**E** and **F**) KCs from WT C57BL/6 (E) or 146a-KO mice (F) were treated with 10 μg/ml HBsAg for 24 h. Relative expression of IL-1β, TNF-α, iNOS, and IL-12a were detected by quantitative real-time PCR. (**G** and **H**) KCs from WT C57BL/6 (G) or 146a-KO mice (H) were pretreated with 10 μg/ml HBsAg or PBS for 24 h, and subsequently treated with 20 ng/ml IFN-γ for 30 min. The Stat1, p-Stat1, and p-I-κB protein levels of KCs were determined with Western blotting. All experiments were repeated three times with similar results. The results are expressed as mean ± SEM of three mice/group. $*p < 0.05$, $**p < 0.01$, by an unpaired two-tailed Student *t* test. AAV, p–AAV-null; AAV-HBV, p–AAV-HBV1.2; 146a-KO, miR-146a$^{-/-}$; Ctrl, control; HBVtg, HBV transgenic; HDI, hydrodynamic injection; WT, wild-type.

IFN-γ–producing CD4$^+$ T cells in clodronate liposome–pretreated mice was significantly higher than that in PBS liposome–pretreated mice (Fig. 4F). These results indicate that KCs induce adaptive immune tolerance to HBV infection, and deficiency of HBV-specific Th1 cell activation may contribute to an impaired antiviral CD8$^+$ T cell response.

To investigate the role of miR-146a–mediated KCs polarization in HBV persistence, miR-146a$^{-/-}$ mice and WT mice were hydrodynamically injected with p-AAV/HBV1.2 plasmid. In the first week after HDI, the levels of serum HBsAg were similar in WT and miR-146a$^{-/-}$ mice, excluding the influence of hepatocellular miR-146a on HBV replication/expression (Fig. 5A). We further examined HBsAg and HBeAg levels in cell culture supernatant following cotransfection of miR-146a inhibitor and pHBV-1.3 plasmid into Huh7 cells. Similar viral expression and replication

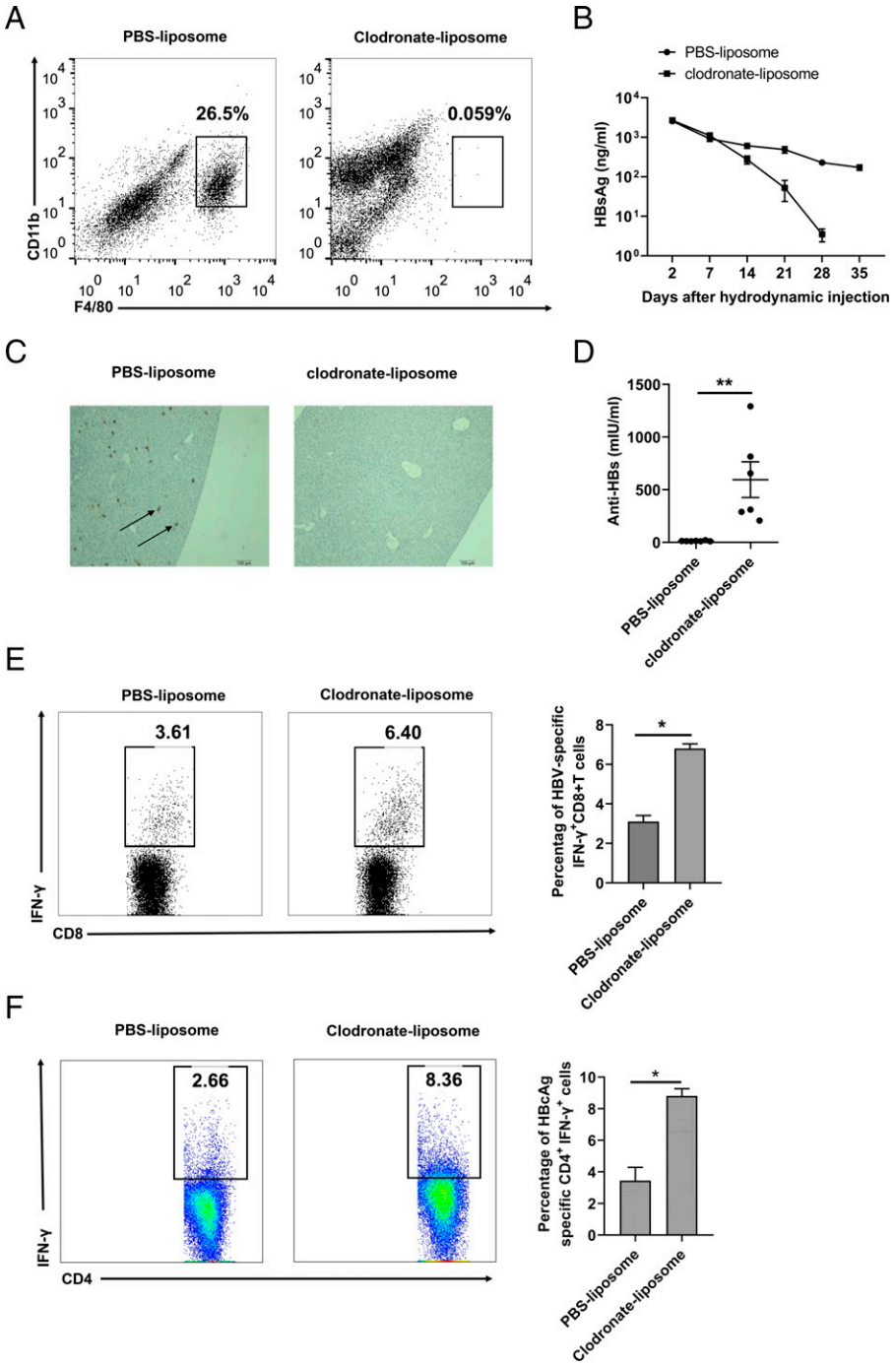

FIGURE 4. Enhanced anti-HBV immune responses in KCs-depleted WT mice. (**A**) C57BL/6 mice were treated with a single i.v. injection of 200 μl of clodronate liposomes or PBS liposomes. The percentage of KCs in hepatic mononuclear cells was detected by flow cytometry 48 h later. (**B–F**) WT C57BL/6 mice received a single i.v. injection of 200 μl of clodronate liposomes or PBS liposomes, followed by HDI of the p–AAV-HBV1.2 plasmid 2 d later. (B) Serum HBsAg levels were examined by ELISA at the indicated time points. (C) Immunostaining of HBcAg in mouse liver 5 wk after HDI. HBcAg is indicated by black arrows. (D) Serum anti-HBs were examined by ELISA 5 wk after HDI. (E) Hepatic lymphocytes were isolated 2 wk after HDI and were then stimulated with 20 μg/ml HBc_{93-100} peptide to analyze the percentage of IFN-γ^+CD8^+ T cells by flow cytometry. (F) Hepatic lymphocytes were isolated as in (E) and were then stimulated with 10 μg/ml HBcAg to analyze the percentage of IFN-γ^+CD4^+ T cells by flow cytometry. All experiments were repeated at least three times. The results are expressed as mean ± SEM of four to five mice/group. *$p < 0.05$, **$p < 0.01$, by an unpaired two-tailed Student t test. 146a-KO, miR-146a$^{-/-}$; anti-HB, anti-HBsAg Ab; HDI, hydrodynamic injection; WT, wild-type.

levels were observed between miR-146a inhibitor- and control-treated cells (data not show), indicating that miR-146a cannot regulate HBV replication in a cell-intrinsic manner. Compared to WT mice, miR-146a$^{-/-}$ mice showed better viral control after HDI, in which serum HBsAg levels (Fig. 5A), HBeAg levels (Fig. 5B, left panel), HBV DNA titers (Fig. 5B, right panel), and hepatocellular HBcAg expression (Fig. 5C) were significantly decreased after HDI. Meanwhile, the percentage of well-characterized K^b-restricted epitope HBc_{93-100}-specific $CD8^+$ T cells in liver detected by HBc_{93-100} tetramer staining increased significantly in miR-146a$^{-/-}$ HBV mice compared with WT HBV mice (5.09 versus 1.89%) (Fig. 5D). Similarly, a significantly increased population of IFN-

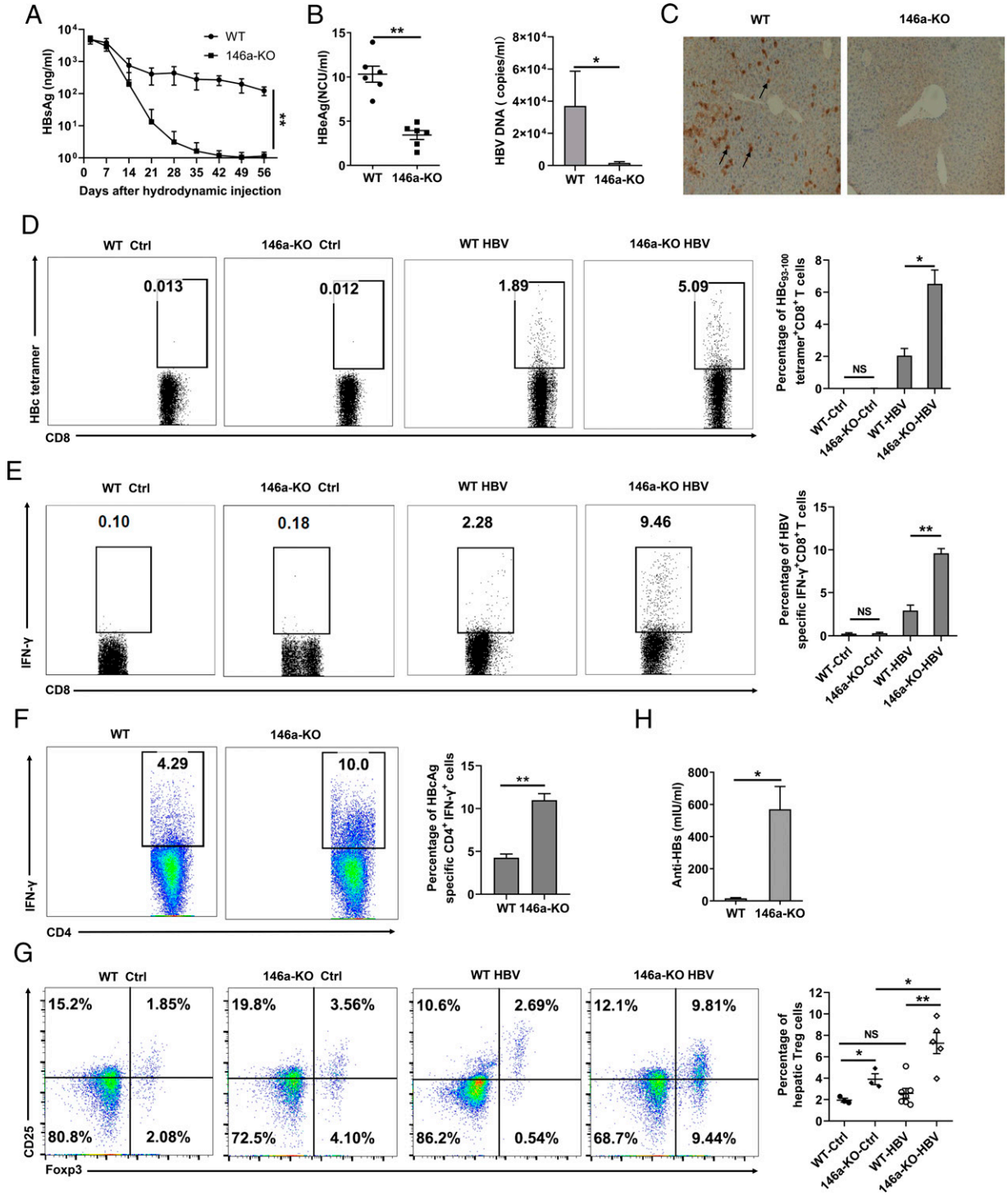

FIGURE 5. miR-146a deficiency promotes HBV clearance and a viral-specific T cell response in an HBV carrier mouse model. (**A**–**H**) WT and 146a-KO C57BL/6 mice were hydrodynamically injected with the p–AAV-HBV1.2 plasmid (A–H) or the p–AAV-null plasmid (control) (D, E, and G). (A) Serum levels of HBsAg were examined by ELISA at the indicated time points. (B) Serum levels of HBeAg and HBV DNA were examined 4 wk after HDI. (C) Immunostaining of HBV core protein (HBcAg) in the liver 5 wk after HDI. HBcAg is indicated by black arrows. (D–G) Hepatic lymphocytes were isolated from mice 2 wk after HDI. (D and E) These cells were then stimulated with 20 μg/ml HBV core peptide (aa 93–100) and analyzed by flow cytometry for percentage of HBc_{93-100} tetramer$^+$CD8$^+$ T cells (D) and IFN-γ$^+$CD8$^+$ T cells (E). (F) Hepatic lymphocytes were stimulated with 10 μg/ml HBcAg and analyzed by flow cytometry for the percentage of HBV-specific IFN-γ$^+$CD4$^+$ T cells. (G) The percentage of CD4$^+$CD25$^+$Foxp3$^+$ Tregs in hepatic lymphocytes was analyzed by flow cytometry. (H) Serum anti-HBs were determined 5 wk after HDI. All experiments were repeated three times. The results are expressed as mean ± SEM of five mice/group. *$p < 0.05$, **$p < 0.01$, by an unpaired two-tailed Student t test. 146a-KO, miR-146a$^{-/-}$; anti-HB, anti-HBsAg Ab; Ctrl, control; HDI, hydrodynamic injection; WT, wild-type.

γ–producing CD8$^+$ T cells was observed in the livers of miR-146a$^{-/-}$ HBV mice (9.46%) when compared with the counterpart in the WT HBV mice (2.28%) (Fig. 5E). Accordingly, the percentage of hepatic IFN-γ–producing CD4$^+$ T cells in miR-146a$^{-/-}$ HBV mice was significantly higher than that in WT HBV mice (Fig. 5F). We also analyzed the proportion of hepatic Tregs in miR-146a$^{-/-}$ and WT mice. As shown in Fig. 5G, the percentage of CD4$^+$CD25$^+$Foxp3$^+$ Tregs in miR-146a$^{-/-}$ HBV mice was

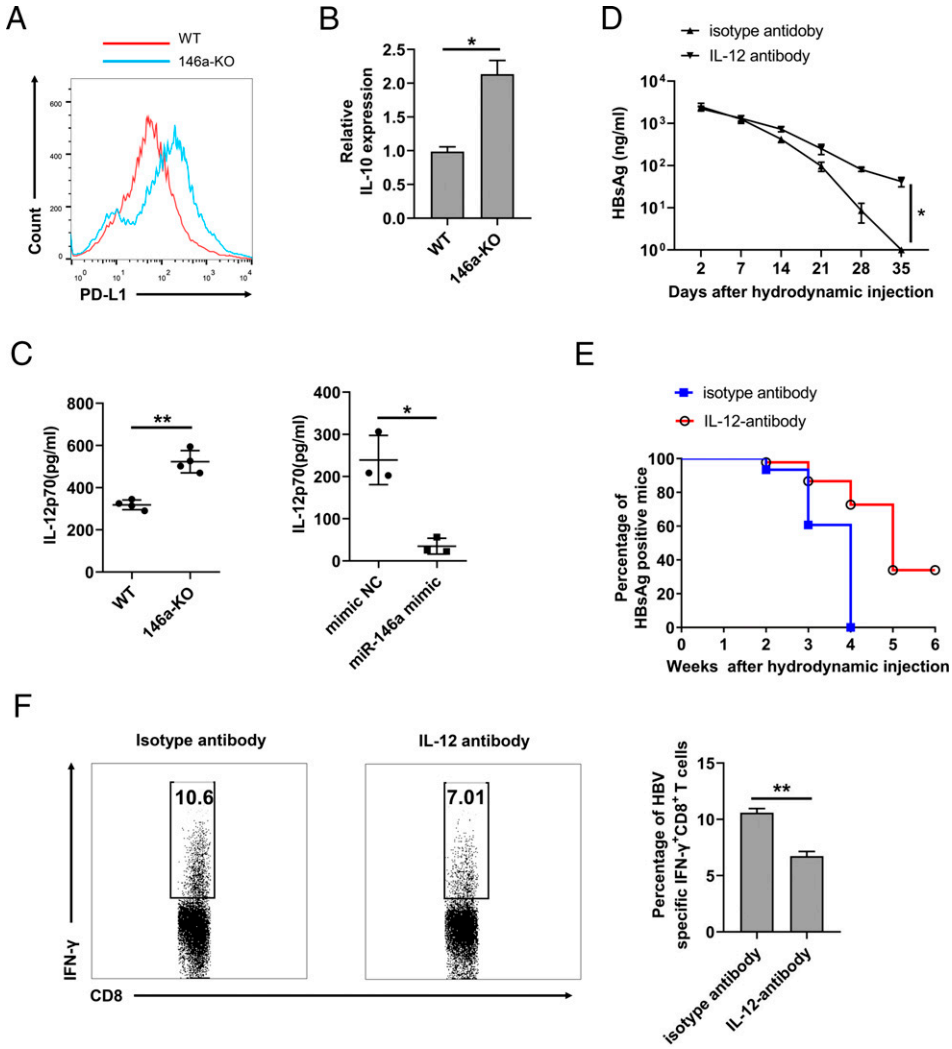

FIGURE 6. Blockade of IL-12 impairs HBV clearance and abolishes specific immune responses in 146a-KO mice. (**A**) The expression of PD-L1 on WT and 146a-KO KCs was analyzed by flow cytometry. (**B**) KCs were isolated from WT and 146a-KO C57BL/6 mice and the relative expression of IL-10 was analyzed by quantitative real-time PCR. (**C**) KCs were isolated from WT and 146a-KO mice and plated in 12-well plates at 10^6 cells/well. Left panel, KCs were treated with 100 ng/ml LPS for 24 h. Right panel, KCs from 146a-KO mice were transfected with miR-146a mimic or mimic control for 24 h and subsequently treated with 100 ng/ml LPS for 24 h. The concentrations of IL-12p75 in the cell culture supernatants were determined by ELISA. The experiment was repeated three times. (**D**–**F**) 146a-KO mice received a single i.p. injection of 1 mg of anti–IL-12p75 or isotype control Ab, followed by HDI of p–AAV-HBV1.2 plasmid 2 d later. The mice were peritoneally injected with 500 μg of anti–IL-12p75 or isotype control Ab on days 2, 7, and 12 after plasmid injection, respectively. (D) Serum HBsAg was examined by ELISA at the indicated time points. (E) Positive rates of serum HBsAg were analyzed. (F) Hepatic lymphocytes were isolated from mice 2 wk after HDI. These cells were then stimulated with 20 μg/ml HBV core peptide (aa 93–100) and the percentage of hepatic HBV-specific $CD8^+$ T cells was analyzed. Experiments in (D)–(F) were repeated twice. Results are expressed as mean ± SEM of five mice/group. $*p < 0.05$, $**p < 0.01$, by an unpaired two-tailed Student *t* test. Log-rank test were used to assess survival. 146a-KO, miR-$146a^{-/-}$; HDI, hydrodynamic injection; WT, wild-type.

significantly higher than that in miR-$146a^{-/-}$ control mice or in WT HBV mice. There was also a moderate increase of Tregs in miR-$146a^{-/-}$ control mice relative to WT control mice. However, the percentage of $CD4^+CD25^+Foxp3^+$ Tregs in WT HBV mice was comparable to that in WT control mice (Fig. 5G). It has been reported that miR-146a deficiency increased Treg expansion, but excessive Stat1 activation due to the loss of miR-146a expression reprogrammed Tregs to Th1-like IFN-γ–secreting cells and impaired their ability to restrict the Th1 response (43). The exact role of Tregs on the KCs-regulated $CD8^+$ T cell response against HBV awaits further investigation. Moreover, high titers of anti-HBs were detected in the sera of miR-$146a^{-/-}$ mice 5 wk after HDI, whereas no Abs were detected in the WT mice (Fig. 5H), indicating that miR-146a deficiency plays a key role in reversing impaired anti-HBV adaptive immunity.

KCs-secreted IL-12 is critical for T cell activation and HBV clearance in miR-146a–deficient mice

Previous studies have shown that increased PD-L1 expression and IL-10 secretion in KCs contribute to HBV persistence in a mouse model (22, 35). However, our results indicated that miR-146a–deficient KCs exhibited higher expression of PD-L1 and IL-10 (Fig. 6A, 6B), which may be the feedback regulation of NF-κB and Stat1 activation. It has been reported that IL-12 plays an important role in viral clearance in CHB (49). The level of IL-12 secreted by miR-$146a^{-/-}$ KCs was significantly higher than that secreted by WT KCs, whereas transfection with the miR-146a mimic resulted in a dramatic decrease in IL-12 secretion (Fig. 6C). As shown in Fig. 6D and 6E, compared with isotype control Ab treatment, continuous IL-12 blockade by anti–IL-12p75 Ab led to increased expression of HBsAg and a higher percentage of HBsAg-positive mice

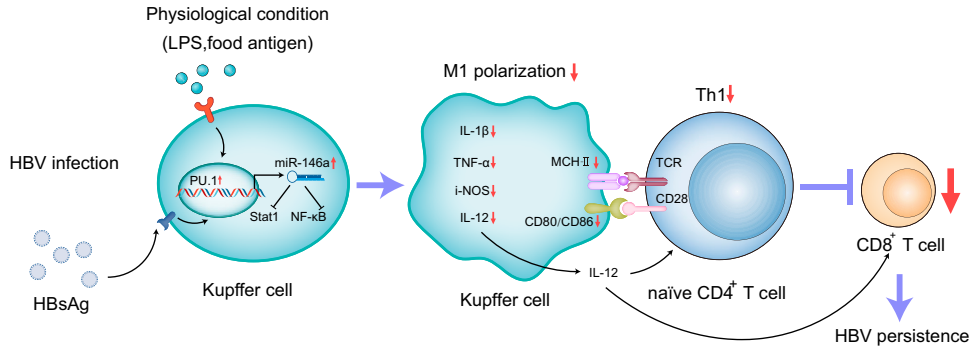

FIGURE 7. Schematic of how the PU.1–miR-146a–Stat1/NF-κB axis may inhibit KCs proinflammatory M1 polarization in the physiological condition and chronic HBV infection. In the physiological condition, the elevated transcription factor PU.1 in KCs induces abundant miR-146a expression, which targets Stat1 and NF-κB and lead to suppression of KCs M1 polarization. Moreover, in chronic HBV infection, the miR-146a expression is further upregulated in KCs by HBsAg-mediated PU.1 accumulation. Subsequently, increased miR-146a leads to further decreased M1 polarization and facilitates immune tolerance to viral infection. In contrast, miR-146a deficiency pronouncedly enhances viral clearance and virus-specific $CD8^+$ T cell immunity.

among the miR-146a$^{-/-}$ mice. In addition, a lower frequency of viral-specific IFN-γ–producing $CD8^+$ T cells was also observed in IL-12–blocked miR-146a$^{-/-}$ mice (Fig. 6F).

Discussion

In this study, by global small RNA sequencing and analysis, we showed substantial expression of miR-146a in KCs via the enrichment of PU.1 to the promoter of miR-146a. Elevated miR-146a expression in KCs decreased M1 polarization by targeting NF-κB and Stat1 and contributed to its immune-tolerant phenotype. Moreover, miR-146a expression was further induced by HBsAg in KCs in HBV-persistent mice, and depletion of KCs enhanced antiviral immunity. miR-146a$^{-/-}$ mice underwent faster recovery and showed stronger immune responses in the HBV carrier mouse model, and increased IL-12 production by miR-146a$^{-/-}$ KCs contributed to the break of immune tolerance. These findings indicate that miR-146a acts as an intrinsic host factor in regulation of KCs polarization and maintenance of an immunosuppressive phenotype, which may be beneficial for maintaining liver immunotolerance and preventing immunopathogenesis under inflammatory stimuli. However, during HBV infection, miR-146a upregulation might dampen immune-mediated viral control and contribute to viral persistence (Fig. 7). According to this model, miR-146a in KCs acts as a critical regulator of immune tolerance in both the physiological condition and chronic HBV infection, supporting the notion that inhibition of miR-146a as a potential therapy for chronic HBV infection.

As a master regulator, a higher PU.1 level is favorable to the development, terminal differentiation, and maturation of macrophages (50). In macrophages, PU.1 functions in nearly whole genome-wide to promote the accessibility of enhancers and cooperates with other transcription factors to establish a distinct enhancer landscape for each tissue-resident macrophage population (51). In the current study, we showed that, under resting conditions, miR-146a expression in KCs was significantly higher than in PMs, which may be partially explained by elevated PU.1 and its increased occupancy at the promoter region of miR-146a. In addition to IFN-γ/LPS, as seen in Figs. 1 and 2, viral pathogen-associated molecular patterns need to be used in in vitro experiments, which may be more relevant to examine how miR-146a changes KCs responses to viral stimuli in the future. In a variety of cells, PU.1 transcription and expression have been shown to be regulated by certain factors, including Runx1, Satb1, NF-like 2, and PU.1 itself (52, 53). KCs exposed to different stimuli may integrate various signals and shape their functional status into a complex and dynamic spectrum of polarization phenotypes. Given that PU.1 controls the global genomic enhancers in macrophages, the mechanism of PU.1 upregulation and its functional role on KCs deserve further investigation.

Abundant research has emphasized the importance of long-term and high-concentration HBsAg stimulation for initiating and maintaining immune tolerance during CHB. HBsAg induces monocytes polarized to an immunosuppressive phenotype with HLA-E, PD-L1, IL-10, and TGF-β upregulation via the MyD88/NF-κB signaling pathway (54). HBsAg can also inhibit antiviral type I IFN production by suppressing major vault protein/MyD88 interaction (55). In addition, HBsAg induces a tolerogenic DCs phenotype characterized by reduced expression of costimulatory molecules and downregulated T cell stimulatory capacity (56). Our results indicated that HBsAg induced the expression of miR-146a by promoting PU.1 accumulation, subsequently altering hepatic macrophage polarization to the immunosuppressive phenotype.

Inadequate innate and adaptive immune responses against HBV are considered to be the main cause of persistent viral infection (57–59). Innate immune cells, especially KCs, are involved in the establishment of CHB infection. Results from an HBV-carrier mouse model suggest that KCs produced abundant inhibitory cytokine IL-10 upon TLR2 interaction with HBcAg (23). The KCs-derived IL-10 cannot only maintain humoral immune tolerance (22) by inducing Tr-1–like cells to inhibit the functions of germinal center B cells and follicular T cells (13), but it also maintains hepatic immune tolerance by directly inhibiting the function of HBV-specific $CD8^+$ T cells (23). Moreover, maternal HBeAg can induce HBV-specific $CD8^+$ T cell exhaustion in offspring by polarizing KCs to a PD-L1 upregulated and M2-like anti-inflammatory phenotype (35). A recent study suggests that KCs from CHB patients expressed higher levels of the anti-inflammatory M2 marker CD163 than those from healthy controls (60). Additionally, ex vivo exposure of naive human KCs to HBV led to less secretion of the proinflammatory cytokine IL-1β, which can inhibit HBV directly (60). Thus, HBV may establish persistent infection in hepatocytes by actively inhibiting antiviral cytokine secretion of KCs. Additionally, KCs also play a critical role in age-dependent dichotomous immunity of HBV infection (61–64). In the current study, we demonstrated that the intrinsic high expression of miR-146a in KCs played a role in maintaining tolerance under homeostasis, and that miR-146a deficiency overcame immune tolerance in an HBV-carrier mouse model, eliciting an increased proportion of HBV-specific IFN-γ^+ $CD8^+$ T cells, IFN-γ^+CD4^+ Th1 cells, and protective levels of anti-HBs. This may partially depend on miR-146a$^{-/-}$ KCs, which develop toward a proinflammatory M1-like phenotype, exhibiting higher

expression of proinflammatory mediators, including TNF-α, IL-1β, and IL-12, and iNOS. Furthermore, miR-146a deficiency enhanced the capacity of KCs to induce proinflammatory $CD4^+$ T cell differentiation involving the upregulation of CD25, CD44, CD69, and Ki-67. Therefore, miR-146a is an important regulator that switches KCs from the proinflammatory state to immune tolerance.

As a negative regulator of the immune response, miR-146a is induced by a broad range of TLRs and cytokine signals and influences the function of many immune cells, including macrophages (39, 65), NK cells (66), germinal center B cells (67), Tregs (43), and Th17 cells (68). Its aberrant expression is associated with many diseases, including viral hepatitis. We previously found that upregulated miR-146a in T cells of CHB dramatically reduced cytotoxicity of $CD4^+$ and $CD8^+$ T cells and inhibited the production of antiviral cytokines via targeting Stat1 (69). Elevated miR-146a expression also contributes to NK cells dysfunction in CHB and hepatocellular carcinoma patients (66). As miR-146a is expressed in a wide range of innate and adaptive immune cell populations, and our miR-146a$^{-/-}$ mice were germ-line knockout, the differences in HBV-specific Th1 cells and $CD8^+$ T responses between WT and miR-146a$^{-/-}$ mice may not specifically be attributed to KCs, but rather to a cumulative effect. Although it has been reported that KCs could prime HBV-specific $CD8^+$ T cells effectively and rescue the dysfunctional $CD8^+$ T cells primed by hepatocytes (8, 47), we cannot rule out the possibility that other hepatic immune cells also play a role in this process. For instance, IL-12 expression and $CD8^+$ T cell activation are classically DCs functions, and silencing miR-146a expression could enhance IL-12 production in DCs (70). It is possible that increased production of IL-12 by miR-146a$^{-/-}$ DCs may also play a role in the T cell activation and HBV clearance in miR-146a$^{-/-}$ mice. The altered function of DCs conferred by miR-146a deficiency requires further study. KCs-specific miR-146a knockout mice may be required for further investigation of its function during chronic HBV infection.

Nevertheless, accelerated HBV clearance was observed upon KCs depletion in WT mice (Fig. 4). In addition to KCs, NKT cells were also partially reduced after clodronate liposome injection (Supplemental Fig. 3A, 3G). Because NKT cells contribute to HBV clearance (71, 72) through sensing of HBV-induced modified self-lipids (73), it is unlikely that NKT cells reduction is involved in the observed enhancement of anti-HBV T cell immunity after clodronate liposome treatment. It is also worthwhile to determine the miR-146a status in human KCs and its potential role in the establishment and maintenance of hepatic immunotolerance in CHB patients, which could further validate its potential as a therapeutic target against HBV infection.

Our current study suggests that KCs with high levels of endogenous miR-146a exhibit an immunosuppressive phenotype and reduce $CD4^+$ and $CD8^+$ T cell responses against HBV. On the one hand, KCs with low levels of CD80, CD86, and MHC-II cannot effectively present viral Ag to $CD4^+$ T cells, resulting in a low response of viral-specific $CD4^+$ T cells. The deficiency in viral-specific Th1 cells can impair CTL development and function (74). On the other hand, KCs suppress the $CD8^+$ T cell response partly by inhibiting the secretion of IL-12, which has been shown to stimulate IFN-γ production by $CD8^+$ T cells and enhance CTL-mediated cytotoxicity (75). Our results imply that KCs may regulate $CD4^+$ and $CD8^+$ T responses through different mechanisms.

In summary, our results highlight that miR-146a, one of the most abundant miRNAs in KCs, is a crucial mediator of macrophage polarization by virtue of its targeting of Stat1 and NF-κB, playing a key role in both the maintenance of liver immune homeostasis and the prevention of viral clearance via immunosuppression in HBV infection. Targeting miR-146a in KCs may have potential utility in the treatment of chronic HBV infection.

Acknowledgments

We thank Prof. Hua Peng (Institute of Biophysics, Chinese Academy of Sciences) for the p-AAV/HBV1.2 plasmid and Prof. Beinan Wang (Institute of Microbiology, Chinese Academy of Sciences) for the OT-II mice. We also thank Tong Zhao (Instrument Sharing Center, Institute of Microbiology, Chinese Academy of Sciences) for help in flow cytometry analysis. We also thank Longchao Liu (Department of Pathology, UT Southwestern Medical Center, Dallas, TX) for precious advise on the establishment of an HBV-persistent mouse model.

Disclosures

The authors have no financial conflicts of interest.

References

1. Crispe, I. N. 2014. Immune tolerance in liver disease. *Hepatology* 60: 2109–2117.
2. Crispe, I. N. 2009. The liver as a lymphoid organ. *Annu. Rev. Immunol.* 27: 147–163.
3. Yuen, M. F., D. S. Chen, G. M. Dusheiko, H. L. A. Janssen, D. T. Y. Lau, S. A. Locarnini, M. G. Peters, and C. L. Lai. 2018. Hepatitis B virus infection. *Nat. Rev. Dis. Primers* 4: 18035.
4. Manns, M. P., M. Buti, E. Gane, J. M. Pawlotsky, H. Razavi, N. Terrault, and Z. Younossi. 2017. Hepatitis C virus infection. *Nat. Rev. Dis. Primers* 3: 17006.
5. Jenne, C. N., and P. Kubes. 2013. Immune surveillance by the liver. *Nat. Immunol.* 14: 996–1006.
6. Bilzer, M., F. Roggel, and A. L. Gerbes. 2006. Role of Kupffer cells in host defense and liver disease. *Liver Int.* 26: 1175–1186.
7. Blériot, C., E. Barreby, G. Dunsmore, R. Ballaire, S. Chakarov, X. Ficht, G. De Simone, F. Andreata, V. Fumagalli, W. Guo, et al. 2021. A subset of Kupffer cells regulates metabolism through the expression of CD36. *Immunity* 54: 2101–2116.e6.
8. De Simone, G., F. Andreata, C. Bleriot, V. Fumagalli, C. Laura, J. M. Garcia-Manteiga, P. Di Lucia, S. Gilotto, X. Ficht, F. F. De Ponti, et al. 2021. Identification of a Kupffer cell subset capable of reverting the T cell dysfunction induced by hepatocellular priming. *Immunity* 54: 2089–2100.e8.
9. Soysa, R., J. C. Bean, X. Wu, S. Lampert, S. Yuen, and I. N. Crispe. 2021. Early-derived murine macrophages temporarily renounce tissue identity during acute systemic inflammation. *J. Immunol.* 207: 569–576.
10. Kanamori, Y., M. Tanaka, M. Itoh, K. Ochi, A. Ito, I. Hidaka, I. Sakaida, Y. Ogawa, and T. Suganami. 2021. Iron-rich Kupffer cells exhibit phenotypic changes during the development of liver fibrosis in NASH. *iScience* 24: 102032.
11. You, Q., L. Cheng, R. M. Kedl, and C. Ju. 2008. Mechanism of T cell tolerance induction by murine hepatic Kupffer cells. *Hepatology* 48: 978–990.
12. Iwai, Y., S. Terawaki, M. Ikegawa, T. Okazaki, and T. Honjo. 2003. PD-1 inhibits antiviral immunity at the effector phase in the liver. *J. Exp. Med.* 198: 39–50.
13. Xu, L., W. Yin, R. Sun, H. Wei, and Z. Tian. 2013. Liver type I regulatory T cells suppress germinal center formation in HBV-tolerant mice. *Proc. Natl. Acad. Sci. USA* 110: 16993–16998.
14. Sun, X., Y. Cui, H. Feng, H. Liu, and X. Liu. 2019. TGF-β signaling controls *Foxp3* methylation and T reg cell differentiation by modulating Uhrf1 activity. *J. Exp. Med.* 216: 2819–2837.
15. Wen, Y., J. Lambrecht, C. Ju, and F. Tacke. 2021. Hepatic macrophages in liver homeostasis and diseases-diversity, plasticity and therapeutic opportunities. *Cell. Mol. Immunol.* 18: 45–56.
16. Murray, P. J. 2017. Macrophage polarization. *Annu. Rev. Physiol.* 79: 541–566.
17. Peng, H., D. Xian, J. Liu, S. Pan, R. Tang, and J. Zhong. 2020. Regulating the polarization of macrophages: a promising approach to vascular dermatosis. *J. Immunol. Res.* 2020: 8148272.
18. Park, J. K., M. Shao, M. Y. Kim, S. K. Baik, M. Y. Cho, T. Utsumi, A. Satoh, X. Ouyang, C. Chung, and Y. Iwakiri. 2017. An endoplasmic reticulum protein, Nogo-B, facilitates alcoholic liver disease through regulation of Kupffer cell polarization. *Hepatology* 65: 1720–1734.
19. Wan, J., M. Benkdane, F. Teixeira-Clerc, S. Bonnafous, A. Louvet, F. Lafdil, F. Pecker, A. Tran, P. Gual, A. Mallat, et al. 2014. M2 Kupffer cells promote M1 Kupffer cell apoptosis: a protective mechanism against alcoholic and nonalcoholic fatty liver disease. *Hepatology* 59: 130–142.
20. Ye, L., S. He, X. Mao, Y. Zhang, Y. Cai, and S. Li. 2020. Effect of hepatic macrophage polarization and apoptosis on liver ischemia and reperfusion injury during liver transplantation. *Front. Immunol.* 11: 1193.
21. Tu, Z., R. H. Pierce, J. Kurtis, Y. Kuroki, I. N. Crispe, and M. S. Orloff. 2010. Hepatitis C virus core protein subverts the antiviral activities of human Kupffer cells. *Gastroenterology* 138: 305–314.
22. Xu, L., W. Yin, R. Sun, H. Wei, and Z. Tian. 2014. Kupffer cell-derived IL-10 plays a key role in maintaining humoral immune tolerance in hepatitis B virus-persistent mice. *Hepatology* 59: 443–452.
23. Li, M., R. Sun, L. Xu, W. Yin, Y. Chen, X. Zheng, Z. Lian, H. Wei, and Z. Tian. 2015. Kupffer cells support hepatitis B virus-mediated $CD8^+$ T cell exhaustion via hepatitis B core antigen-TLR2 interactions in mice. *J. Immunol.* 195: 3100–3109.
24. Ghosh, Z., B. Mallick, and J. Chakrabarti. 2009. Cellular versus viral microRNAs in host-virus interaction. *Nucleic Acids Res.* 37: 1035–1048.
25. Curtis, A. M., C. T. Fagundes, G. Yang, E. M. Palsson-McDermott, P. Wochal, A. F. McGettrick, N. H. Foley, J. O. Early, L. Chen, H. Zhang, et al. 2015. Circadian control

of innate immunity in macrophages by miR-155 targeting *Bmal1*. *Proc. Natl. Acad. Sci. USA* 112: 7231–7236.
26. O'Connell, R. M., K. D. Taganov, M. P. Boldin, G. Cheng, and D. Baltimore. 2007. MicroRNA-155 is induced during the macrophage inflammatory response. *Proc. Natl. Acad. Sci. USA* 104: 1604–1609.
27. Cichocki, F., M. Felices, V. McCullar, S. R. Presnell, A. Al-Attar, C. T. Lutz, and J. S. Miller. 2011. Cutting edge: microRNA-181 promotes human NK cell development by regulating Notch signaling. *J. Immunol.* 187: 6171–6175.
28. Moffett, H. F., A. N. R. Cartwright, H. J. Kim, J. Godec, J. Pyrdol, T. Äijö, G. J. Martinez, A. Rao, J. Lu, T. R. Golub, et al. 2017. The microRNA miR-31 inhibits $CD8^+$ T cell function in chronic viral infection. [Published erratum appears in 2017 *Nat. Immunol.* 18: 1173.] *Nat. Immunol.* 18: 791–799.
29. Li, Z., S. Zhang, Y. Wan, M. Cai, W. Wang, Y. Zhu, Z. Li, Y. Hu, H. Wang, H. Chen, et al. 2018. MicroRNA-146a overexpression impairs the positive selection during T cell development. *Front. Immunol.* 8: 2006.
30. Li, Q. J., J. Chau, P. J. Ebert, G. Sylvester, H. Min, G. Liu, R. Braich, M. Manoharan, J. Soutschek, P. Skare, et al. 2007. miR-181a is an intrinsic modulator of T cell sensitivity and selection. *Cell* 129: 147–161.
31. Huang, L. R., H. L. Wu, P. J. Chen, and D. S. Chen. 2006. An immunocompetent mouse model for the tolerance of human chronic hepatitis B virus infection. *Proc. Natl. Acad. Sci. USA* 103: 17862–17867.
32. Moreno, S. G. 2018. Depleting macrophages in vivo with clodronate-liposomes. *Methods Mol. Biol.* 1784: 259–262.
33. Aparicio-Vergara, M., M. Tencerova, C. Morgantini, E. Barreby, and M. Aouadi. 2017. Isolation of Kupffer cells and hepatocytes from a single mouse liver. *Methods Mol. Biol.* 1639: 161–171.
34. Liu, J., X. Huang, M. Werner, R. Broering, D. Yang, and M. Lu. 2017. Advanced method for isolation of mouse hepatocytes, liver sinusoidal endothelial cells, and Kupffer cells. *Methods Mol. Biol.* 1540: 249–258.
35. Tian, Y., C. F. Kuo, O. Akbari, and J. H. Ou. 2016. Maternal-derived hepatitis B virus e antigen alters macrophage function in offspring to drive viral persistence after vertical transmission. *Immunity* 44: 1204–1214.
36. Wang, J., R. Sun, H. Wei, Z. Dong, B. Gao, and Z. Tian. 2006. Poly I:C prevents T cell-mediated hepatitis via an NK-dependent mechanism. *J. Hepatol.* 44: 446–454.
37. Ye, C., X. Zhang, J. Wan, L. Chang, W. Hu, Z. Bing, S. Zhang, J. Li, J. He, J. Wang, and G. Zhou, et al. 2013. Radiation-induced cellular senescence results from a slippage of long-term G2 arrested cells into G1 phase. *Cell Cycle* 12: 1424–1432.
38. Movita, D., K. Kreefft, P. Biesta, A. van Oudenaren, P. J. Leenen, H. L. Janssen, and A. Boonstra. 2012. Kupffer cells express a unique combination of phenotypic and functional characteristics compared with splenic and peritoneal macrophages. *J. Leukoc. Biol.* 92: 723–733.
39. Taganov, K. D., M. P. Boldin, K. J. Chang, and D. Baltimore. 2006. NF-κB-dependent induction of microRNA miR-146, an inhibitor targeted to signaling proteins of innate immune responses. *Proc. Natl. Acad. Sci. USA* 103: 12481–12486.
40. Luo, X., W. Yang, D. Q. Ye, H. Cui, Y. Zhang, N. Hirankarn, X. Qian, Y. Tang, Y. L. Lau, N. de Vries, et al. 2011. A functional variant in microRNA-146a promoter modulates its expression and confers disease risk for systemic lupus erythematosus. *PLoS Genet.* 7: e1002128.
41. Ghani, S., P. Riemke, J. Schönheit, D. Lenze, J. Stumm, M. Hoogenkamp, A. Lagendijk, S. Heinz, C. Bonifer, J. Bakkers, et al. 2011. Macrophage development from HSCs requires PU.1-coordinated microRNA expression. *Blood* 118: 2275–2284.
42. Huang, C., X. J. Liu, J. QunZhou, T. T. Xie, X. M. Ma, Meng, and J. Li. 2016. miR-146a modulates macrophage polarization by inhibiting Notch1 pathway in RAW264.7 macrophages. *Int. Immunopharmacol.* 32: 46–54.
43. Lu, L. F., M. P. Boldin, A. Chaudhry, L. L. Lin, K. D. Taganov, T. Hanada, A. Yoshimura, D. Baltimore, and A. Y. Rudensky. 2010. Function of miR-146a in controlling Treg cell-mediated regulation of Th1 responses. *Cell* 142: 914–929.
44. Wang, S., L. Qiu, G. Liu, Y. Li, X. Zhang, W. Jin, G. F. Gao, X. Kong, and S. Meng. 2011. Heat shock protein gp96 enhances humoral and T cell responses, decreases Treg frequency and potentiates the anti-HBV activity in BALB/c and transgenic mice. *Vaccine* 29: 6342–6351.
45. Van Rooijen, N., and A. Sanders. 1996. Kupffer cell depletion by liposome-delivered drugs: comparative activity of intracellular clodronate, propamidine, and ethylenediaminetetraacetic acid. *Hepatology* 23: 1239–1243.
46. Sitia, G., M. Iannacone, R. Aiolfi, M. Isogawa, N. van Rooijen, C. Scozzesi, M. E. Bianchi, U. H. von Andrian, F. V. Chisari, and L. G. Guidotti. 2011. Kupffer cells hasten resolution of liver immunopathology in mouse models of viral hepatitis. *PLoS Pathog.* 7: e1002061.
47. Bénéchet, A. P., G. De Simone, P. Di Lucia, F. Cilenti, G. Barbiera, N. Le Bert, V. Fumagalli, E. Lusito, F. Moalli, V. Bianchessi, et al. 2019. Dynamics and genomic landscape of $CD8^+$ T cells undergoing hepatic priming. *Nature* 574: 200–205.
48. Cui, K., G. Yan, C. Xu, Y. Chen, J. Wang, R. Zhou, L. Bai, Z. Lian, H. Wei, R. Sun, and Z. Tian. 2015. Invariant NKT cells promote alcohol-induced steatohepatitis through interleukin-1β in mice. *J. Hepatol.* 62: 1311–1318.
49. Rossol, S., G. Marinos, P. Carucci, M. V. Singer, R. Williams, and N. V. Naoumov. 1997. Interleukin-12 induction of Th1 cytokines is important for viral clearance in chronic hepatitis B. *J. Clin. Invest.* 99: 3025–3033.
50. Kueh, H. Y., A. Champhekar, S. L. Nutt, M. B. Elowitz, and E. V. Rothenberg. 2013. Positive feedback between PU.1 and the cell cycle controls myeloid differentiation. [Published erratum appears in 2013 *Science* 342: 311.] *Science* 341: 670–673.
51. Lavin, Y., D. Winter, R. Blecher-Gonen, E. David, H. Keren-Shaul, M. Merad, S. Jung, and I. Amit. 2014. Tissue-resident macrophage enhancer landscapes are shaped by the local microenvironment. *Cell* 159: 1312–1326.
52. Willcockson, M. A., S. J. Taylor, S. Ghosh, S. E. Healton, J. C. Wheat, T. J. Wilson, U. Steidl, and A. I. Skoultchi. 2019. Runx1 promotes murine erythroid progenitor proliferation and inhibits differentiation by preventing Pu.1 downregulation. *Proc. Natl. Acad. Sci. USA* 116: 17841–17847.
53. Staitieh, B. S., X. Fan, W. Neveu, and D. M. Guidot. 2015. Nrf2 regulates PU.1 expression and activity in the alveolar macrophage. *Am. J. Physiol. Lung Cell. Mol. Physiol.* 308: L1086–L1093.
54. Li, H., N. Zhai, Z. Wang, H. Song, Y. Yang, A. Cui, T. Li, G. Wang, J. Niu, I. N. Crispe, et al. 2018. Regulatory NK cells mediated between immunosuppressive monocytes and dysfunctional T cells in chronic HBV infection. *Gut* 67: 2035–2044.
55. Liu, S., N. Peng, J. Xie, Q. Hao, M. Zhang, Y. Zhang, Z. Xia, G. Xu, F. Zhao, Q. Wang, et al. 2015. Human hepatitis B virus surface and e antigens inhibit major vault protein signaling in interferon induction pathways. *J. Hepatol.* 62: 1015–1023.
56. Op den Brouw, M. L., R. S. Binda, M. H. van Roosmalen, U. Protzer, H. L. Janssen, R. G. van der Molen, and A. M. Woltman. 2009. Hepatitis B virus surface antigen impairs myeloid dendritic cell function: a possible immune escape mechanism of hepatitis B virus. *Immunology* 126: 280–289.
57. Bengsch, B., B. Martin, and R. Thimme. 2014. Restoration of HBV-specific $CD8^+$ T cell function by PD-1 blockade in inactive carrier patients is linked to T cell differentiation. *J. Hepatol.* 61: 1212–1219.
58. Bertoletti, A., and C. Ferrari. 2016. Adaptive immunity in HBV infection. *J. Hepatol.* 64(1, Suppl): S71–S83.
59. Wherry, E. J. 2011. T cell exhaustion. *Nat. Immunol.* 12: 492–499.
60. Faure-Dupuy, S., M. Delphin, L. Aillot, L. Dimier, F. Lebossé, J. Fresquet, R. Parent, M. S. Matter, M. Rivoire, N. Bendriss-Vermare, et al. 2019. Hepatitis B virus-induced modulation of liver macrophage function promotes hepatocyte infection. *J. Hepatol.* 71: 1086–1098.
61. Publicover, J., A. Gaggar, S. Nishimura, C. M. Van Horn, A. Goodsell, M. O. Muench, R. L. Reinhardt, N. van Rooijen, A. E. Wakil, M. Peters, et al. 2013. Age-dependent hepatic lymphoid organization directs successful immunity to hepatitis B. *J. Clin. Invest.* 123: 3728–3739.
62. Publicover, J., A. Gaggar, J. M. Jespersen, U. Halac, A. J. Johnson, A. Goodsell, L. Avanesyan, S. L. Nishimura, M. Holdorf, K. G. Mansfield, et al. 2018. An OX40/OX40L interaction directs successful immunity to hepatitis B virus. *Sci. Transl. Med.* 10: eaah5766.
63. Chou, H. H., W. H. Chien, L. L. Wu, C. H. Cheng, C. H. Chung, J. H. Horng, Y. H. Ni, H. T. Tseng, D. Wu, X. Lu, et al. 2015. Age-related immune clearance of hepatitis B virus infection requires the establishment of gut microbiota. *Proc. Natl. Acad. Sci. USA* 112: 2175–2180.
64. Wu, L. L., W. H. Peng, H. L. Wu, S. C. Miaw, S. H. Yeh, H. C. Yang, P. H. Liao, J. S. Lin, Y. R. Chen, Y. T. Hong, et al. 2019. Lymphocyte antigen 6 complex, locus C^+ monocytes and Kupffer cells orchestrate liver immune responses against hepatitis B virus in mice. *Hepatology* 69: 2364–2380.
65. Boldin, M. P., K. D. Taganov, D. S. Rao, L. Yang, J. L. Zhao, M. Kalwani, Y. Garcia-Flores, M. Luong, A. Devrekanli, J. Xu, et al. 2011. miR-146a is a significant brake on autoimmunity, myeloproliferation, and cancer in mice. *J. Exp. Med.* 208: 1189–1201.
66. Xu, D., Q. Han, Z. Hou, C. Zhang, and J. Zhang. 2017. miR-146a negatively regulates NK cell functions via STAT1 signaling. *Cell. Mol. Immunol.* 14: 712–720.
67. Cho, S., H. M. Lee, I. S. Yu, Y. S. Choi, H. Y. Huang, S. S. Hashemifar, L. L. Lin, M. C. Chen, N. D. Afanasiev, A. A. Khan, et al. 2018. Differential cell-intrinsic regulations of germinal center B and T cells by miR-146a and miR-146b. *Nat. Commun.* 9: 2757.
68. Li, B., X. Wang, I. Y. Choi, Y. C. Wang, S. Liu, A. T. Pham, H. Moon, D. J. Smith, D. S. Rao, M. P. Boldin, and L. Yang. 2017. miR-146a modulates autoreactive Th17 cell differentiation and regulates organ-specific autoimmunity. *J. Clin. Invest.* 127: 3702–3716.
69. Wang, S., X. Zhang, Y. Ju, B. Zhao, X. Yan, J. Hu, L. Shi, L. Yang, Z. Ma, L. Chen, et al. 2013. MicroRNA-146a feedback suppresses T cell immune function by targeting Stat1 in patients with chronic hepatitis B. *J. Immunol.* 191: 293–301.
70. Park, H., X. Huang, C. Lu, M. S. Cairo, and X. Zhou. 2015. MicroRNA-146a and microRNA-146b regulate human dendritic cell apoptosis and cytokine production by targeting TRAF6 and IRAK1 proteins. *J. Biol. Chem.* 290: 2831–2841.
71. Baron, J. L., L. Gardiner, S. Nishimura, K. Shinkai, R. Locksley, and D. Ganem. 2002. Activation of a nonclassical NKT cell subset in a transgenic mouse model of hepatitis B virus infection. *Immunity* 16: 583–594.
72. Kakimi, K., L. G. Guidotti, Y. Koezuka, and F. V. Chisari. 2000. Natural killer T cell activation inhibits hepatitis B virus replication in vivo. *J. Exp. Med.* 192: 921–930.
73. Zeissig, S., K. Murata, L. Sweet, J. Publicover, Z. Hu, A. Kaser, E. Bosse, J. Iqbal, M. M. Hussain, K. Balschun, et al. 2012. Hepatitis B virus-induced lipid alterations contribute to natural killer T cell-dependent protective immunity. *Nat. Med.* 18: 1060–1068.
74. Chen, W., M. Shi, F. Shi, Y. Mao, Z. Tang, B. Zhang, H. Zhang, L. Chen, L. Chen, S. Xin, and F. S. Wang. 2009. HBcAg-pulsed dendritic cell vaccine induces Th1 polarization and production of hepatitis B virus-specific cytotoxic T lymphocytes. *Hepatol. Res.* 39: 355–365.
75. Beadling, C., and M. K. Slifka. 2005. Differential regulation of virus-specific T-cell effector functions following activation by peptide or innate cytokines. *Blood* 105: 1179–1186.